

Study of $e^+e^- \rightarrow \pi^+\pi^-\pi^0$ process using initial state radiation with *BABAR*

B. Aubert, R. Barate, D. Boutigny, F. Couderc, J.-M. Gaillard,
A. Hicheur, Y. Karyotakis, J. P. Lees, V. Tisserand, and A. Zghiche
Laboratoire de Physique des Particules, F-74941 Annecy-le-Vieux, France

A. Palano and A. Pompili
Università di Bari, Dipartimento di Fisica and INFN, I-70126 Bari, Italy

J. C. Chen, N. D. Qi, G. Rong, P. Wang, and Y. S. Zhu
Institute of High Energy Physics, Beijing 100039, China

G. Eigen, I. Ofte, and B. Stugu
University of Bergen, Inst. of Physics, N-5007 Bergen, Norway

G. S. Abrams, A. W. Borgland, A. B. Breon, D. N. Brown, J. Button-Shafer, R. N. Cahn,
E. Charles, C. T. Day, M. S. Gill, A. V. Gritsan, Y. Groysman, R. G. Jacobsen, R. W. Kadel,
J. Kadyk, L. T. Kerth, Yu. G. Kolomensky, G. Kukartsev, G. Lynch, L. M. Mir, P. J. Oddone,
T. J. Orimoto, M. Pripstein, N. A. Roe, M. T. Ronan, V. G. Shelkov, and W. A. Wenzel
Lawrence Berkeley National Laboratory and University of California, Berkeley, CA 94720, USA

M. Barrett, K. E. Ford, T. J. Harrison, A. J. Hart, C. M. Hawkes, S. E. Morgan, and A. T. Watson
University of Birmingham, Birmingham, B15 2TT, United Kingdom

M. Fritsch, K. Goetzen, T. Held, H. Koch, B. Lewandowski, M. Pelizaeus, and M. Steinke
Ruhr Universität Bochum, Institut für Experimentalphysik 1, D-44780 Bochum, Germany

J. T. Boyd, N. Chevalier, W. N. Cottingham, M. P. Kelly, T. E. Latham, and F. F. Wilson
University of Bristol, Bristol BS8 1TL, United Kingdom

T. Cuhadar-Donszelmann, C. Hearty, N. S. Knecht, T. S. Mattison, J. A. McKenna, and D. Thiessen
University of British Columbia, Vancouver, BC, Canada V6T 1Z1

A. Khan, P. Kyberd, and L. Teodorescu
Brunel University, Uxbridge, Middlesex UB8 3PH, United Kingdom

A. E. Blinov, V. E. Blinov, V. P. Druzhinin, V. B. Golubev, V. N. Ivanchenko, E. A. Kravchenko,
A. P. Onuchin, S. I. Serednyakov, Yu. I. Skovpen, E. P. Solodov, and A. N. Yushkov
Budker Institute of Nuclear Physics, Novosibirsk 630090, Russia

D. Best, M. Bruinsma, M. Chao, I. Eschrich, D. Kirkby, A. J. Lankford,
M. Mandelkern, R. K. Mommsen, W. Roethel, and D. P. Stoker
University of California at Irvine, Irvine, CA 92697, USA

C. Buchanan and B. L. Hartfiel
University of California at Los Angeles, Los Angeles, CA 90024, USA

S. D. Foulkes, J. W. Gary, B. C. Shen, and K. Wang
University of California at Riverside, Riverside, CA 92521, USA

D. del Re, H. K. Hadavand, E. J. Hill, D. B. MacFarlane, H. P. Paar, Sh. Rahatlou, and V. Sharma
University of California at San Diego, La Jolla, CA 92093, USA

J. W. Berryhill, C. Campagnari, B. Dahmes, O. Long, A. Lu, M. A. Mazur, J. D. Richman, and W. Verkerke
University of California at Santa Barbara, Santa Barbara, CA 93106, USA

T. W. Beck, A. M. Eisner, C. A. Heusch, J. Kroseberg, W. S. Lockman, G. Nesom,

T. Schalk, B. A. Schumm, A. Seiden, P. Spradlin, D. C. Williams, and M. G. Wilson
University of California at Santa Cruz, Institute for Particle Physics, Santa Cruz, CA 95064, USA

J. Albert, E. Chen, G. P. Dubois-Felsmann, A. Dvoretzskii, D. G. Hitlin,
 I. Narsky, T. Piatenko, F. C. Porter, A. Ryd, A. Samuel, and S. Yang
California Institute of Technology, Pasadena, CA 91125, USA

S. Jayatilke, G. Mancinelli, B. T. Meadows, and M. D. Sokoloff
University of Cincinnati, Cincinnati, OH 45221, USA

T. Abe, F. Blanc, P. Bloom, S. Chen, W. T. Ford, U. Nauenberg,
 A. Olivas, P. Rankin, J. G. Smith, J. Zhang, and L. Zhang
University of Colorado, Boulder, CO 80309, USA

A. Chen, J. L. Harton, A. Soffer, W. H. Toki, R. J. Wilson, and Q. L. Zeng
Colorado State University, Fort Collins, CO 80523, USA

D. Altenburg, T. Brandt, J. Brose, M. Dickopp, E. Feltresi, A. Hauke, H. M. Lacker, R. Müller-Pfefferkorn,
 R. Nogowski, S. Otto, A. Petzold, J. Schubert, K. R. Schubert, R. Schwierz, B. Spaan, and J. E. Sundermann
Technische Universität Dresden, Institut für Kern- und Teilchenphysik, D-01062 Dresden, Germany

D. Bernard, G. R. Bonneaud, F. Brochard, P. Grenier, S. Schrenk, Ch. Thiebaux, G. Vasileiadis, and M. Verderi
Ecole Polytechnique, LLR, F-91128 Palaiseau, France

D. J. Bard, P. J. Clark, D. Lavin, F. Muheim, S. Playfer, and Y. Xie
University of Edinburgh, Edinburgh EH9 3JZ, United Kingdom

M. Andreotti, V. Azzolini, D. Bettoni, C. Bozzi, R. Calabrese,
 G. Cibinetto, E. Luppi, M. Negrini, L. Piemontese, and A. Sarti
Università di Ferrara, Dipartimento di Fisica and INFN, I-44100 Ferrara, Italy

E. Treadwell
Florida A&M University, Tallahassee, FL 32307, USA

F. Anulli, R. Baldini-Ferrolì, A. Calcaterra, R. de Sangro,
 G. Finocchiaro, P. Patteri, I. M. Peruzzi, M. Piccolo, and A. Zallo
Laboratori Nazionali di Frascati dell'INFN, I-00044 Frascati, Italy

A. Buzzo, R. Capra, R. Contri, G. Crosetti, M. Lo Vetere, M. Macri,
 M. R. Monge, S. Passaggio, C. Patrignani, E. Robutti, A. Santroni, and S. Tosi
Università di Genova, Dipartimento di Fisica and INFN, I-16146 Genova, Italy

S. Bailey, G. Brandenburg, K. S. Chaisanguanthum, M. Morii, and E. Won
Harvard University, Cambridge, MA 02138, USA

R. S. Dubitzky and U. Langenegger
Universität Heidelberg, Physikalisches Institut, Philosophenweg 12, D-69120 Heidelberg, Germany

W. Bhimji, D. A. Bowerman, P. D. Dauncey, U. Egede, J. R. Gaillard,
 G. W. Morton, J. A. Nash, M. B. Nikolich, and G. P. Taylor
Imperial College London, London, SW7 2AZ, United Kingdom

M. J. Charles, G. J. Grenier, and U. Mallik
University of Iowa, Iowa City, IA 52242, USA

J. Cochran, H. B. Crawley, J. Lamsa, W. T. Meyer, S. Prell, E. I. Rosenberg, A. E. Rubin, and J. Yi
Iowa State University, Ames, IA 50011-3160, USA

M. Biasini, R. Covarelli, and M. Pioppi
Università di Perugia, Dipartimento di Fisica and INFN, I-06100 Perugia, Italy

M. Davier, X. Giroux, G. Grosdidier, A. Höcker, S. Laplace, F. Le Diberder, V. Lepeltier,
 A. M. Lutz, T. C. Petersen, S. Plaszczynski, M. H. Schune, L. Tantot, and G. Wormser
Laboratoire de l'Accélérateur Linéaire, F-91898 Orsay, France

C. H. Cheng, D. J. Lange, M. C. Simani, and D. M. Wright
Lawrence Livermore National Laboratory, Livermore, CA 94550, USA

A. J. Bevan, C. A. Chavez, J. P. Coleman, I. J. Forster, J. R. Fry, E. Gabathuler,
 R. Gamet, D. E. Hutchcroft, R. J. Parry, D. J. Payne, R. J. Sloane, and C. Touramanis
University of Liverpool, Liverpool L69 72E, United Kingdom

J. J. Back,* C. M. Cormack, P. F. Harrison,* F. Di Lodovico, and G. B. Mohanty*
Queen Mary, University of London, E1 4NS, United Kingdom

C. L. Brown, G. Cowan, R. L. Flack, H. U. Flaecher, M. G. Green,
 P. S. Jackson, T. R. McMahon, S. Ricciardi, F. Salvatore, and M. A. Winter
University of London, Royal Holloway and Bedford New College, Egham, Surrey TW20 0EX, United Kingdom

D. Brown and C. L. Davis
University of Louisville, Louisville, KY 40292, USA

J. Allison, N. R. Barlow, R. J. Barlow, P. A. Hart, M. C. Hodgkinson, G. D. Lafferty, A. J. Lyon, and J. C. Williams
University of Manchester, Manchester M13 9PL, United Kingdom

A. Farbin, W. D. Hulsbergen, A. Jawahery, D. Kovalskyi, C. K. Lae, V. Lillard, and D. A. Roberts
University of Maryland, College Park, MD 20742, USA

G. Blaylock, C. Dallapiccola, K. T. Flood, S. S. Hertzbach, R. Kofler,
 V. B. Koptchev, T. B. Moore, S. Saremi, H. Staengle, and S. Willocq
University of Massachusetts, Amherst, MA 01003, USA

R. Cowan, G. Sciolla, S. J. Sekula, F. Taylor, and R. K. Yamamoto
Massachusetts Institute of Technology, Laboratory for Nuclear Science, Cambridge, MA 02139, USA

D. J. J. Mangeol, P. M. Patel, and S. H. Robertson
McGill University, Montréal, QC, Canada H3A 2T8

A. Lazzaro, V. Lombardo, and F. Palombo
Università di Milano, Dipartimento di Fisica and INFN, I-20133 Milano, Italy

J. M. Bauer, L. Cremaldi, V. Eschenburg, R. Godang, R. Kroeger,
 J. Reidy, D. A. Sanders, D. J. Summers, and H. W. Zhao
University of Mississippi, University, MS 38677, USA

S. Brunet, D. Côté, and P. Taras
Université de Montréal, Laboratoire René J. A. Lévesque, Montréal, QC, Canada H3C 3J7

H. Nicholson
Mount Holyoke College, South Hadley, MA 01075, USA

N. Cavallo,[†] F. Fabozzi,[†] C. Gatto, L. Lista, D. Monorchio, P. Paolucci, D. Piccolo, and C. Sciacca
Università di Napoli Federico II, Dipartimento di Scienze Fisiche and INFN, I-80126, Napoli, Italy

M. Baak, H. Bulten, G. Raven, H. L. Snoek, and L. Wilden
NIKHEF, National Institute for Nuclear Physics and High Energy Physics, NL-1009 DB Amsterdam, The Netherlands

C. P. Jessop and J. M. LoSecco
University of Notre Dame, Notre Dame, IN 46556, USA

T. Allmendinger, K. K. Gan, K. Honscheid, D. Hufnagel, H. Kagan,
 R. Kass, T. Pulliam, A. M. Rahimi, R. Ter-Antonyan, and Q. K. Wong
Ohio State University, Columbus, OH 43210, USA

J. Brau, R. Frey, O. Igonkina, C. T. Potter, N. B. Sinev, D. Strom, and E. Torrence
University of Oregon, Eugene, OR 97403, USA

F. Colechia, A. Dorigo, F. Galeazzi, M. Margoni, M. Morandin,
 M. Posocco, M. Rotondo, F. Simonetto, R. Stroili, G. Tiozzo, and C. Voci
Università di Padova, Dipartimento di Fisica and INFN, I-35131 Padova, Italy

M. Benayoun, H. Briand, J. Chauveau, P. David, Ch. de la Vaissière, L. Del Buono, O. Hamon,
 M. J. J. John, Ph. Leruste, J. Malcles, J. Ocariz, M. Pivk, L. Roos, S. T'Jampens, and G. Therin
Universités Paris VI et VII, Laboratoire de Physique Nucléaire et de Hautes Energies, F-75252 Paris, France

P. F. Manfredi and V. Re
Università di Pavia, Dipartimento di Eletttronica and INFN, I-27100 Pavia, Italy

P. K. Behera, L. Gladney, Q. H. Guo, and J. Panetta
University of Pennsylvania, Philadelphia, PA 19104, USA

C. Angelini, G. Batignani, S. Bettarini, M. Bondioli, F. Bucci, G. Calderini,
 M. Carpinelli, F. Forti, M. A. Giorgi, A. Lusiani, G. Marchiori, F. Martinez-Vidal,[‡]
 M. Morganti, N. Neri, E. Paoloni, M. Rama, G. Rizzo, F. Sandrelli, and J. Walsh
Università di Pisa, Dipartimento di Fisica, Scuola Normale Superiore and INFN, I-56127 Pisa, Italy

M. Haire, D. Judd, K. Paick, and D. E. Wagoner
Prairie View A&M University, Prairie View, TX 77446, USA

N. Danielson, P. Elmer, Y. P. Lau, C. Lu, V. Miftakov, J. Olsen, A. J. S. Smith, and A. V. Telnov
Princeton University, Princeton, NJ 08544, USA

F. Bellini, R. Faccini, F. Ferrarotto, F. Ferroni, M. Gaspero, L. Li Gioi,
 M. A. Mazzoni, S. Morganti, M. Pierini, G. Piredda, F. Safai Tehrani, and C. Voena
Università di Roma La Sapienza, Dipartimento di Fisica and INFN, I-00185 Roma, Italy

G. Cavoto
Princeton University, Princeton, NJ 08544, USA and
Università di Roma La Sapienza, Dipartimento di Fisica and INFN, I-00185 Roma, Italy

S. Christ, G. Wagner, and R. Waldi
Universität Rostock, D-18051 Rostock, Germany

T. Adye, N. De Groot, B. Franek, N. I. Geddes, G. P. Gopal, and E. O. Olaiya
Rutherford Appleton Laboratory, Chilton, Didcot, Oxon, OX11 0QX, United Kingdom

R. Aleksan, S. Emery, A. Gaidot, S. F. Ganzhur, P.-F. Giraud, G. Hamel de Monchenault,
 W. Kozanecki, M. Legendre, G. W. London, B. Mayer, G. Schott, G. Vasseur, Ch. Yèche, and M. Zito
DSM/Daphnia, CEA/Saclay, F-91191 Gif-sur-Yvette, France

M. V. Purohit, A. W. Weidemann, J. R. Wilson, and F. X. Yumiceva
University of South Carolina, Columbia, SC 29208, USA

D. Aston, R. Bartoldus, N. Berger, A. M. Boyarski, O. L. Buchmueller, R. Claus, M. R. Convery, M. Cristinziani,

G. De Nardo, D. Dong, J. Dorfan, D. Dujmic, W. Dunwoodie, E. E. Elsen, S. Fan, R. C. Field, T. Glanzman, S. J. Gowdy, T. Hadig, V. Halyo, C. Hast, T. Hryn'ova, W. R. Innes, M. H. Kelsey, P. Kim, M. L. Kocian, D. W. G. S. Leith, J. Libby, S. Luitz, V. Luth, H. L. Lynch, H. Marsiske, R. Messner, D. R. Muller, C. P. O'Grady, V. E. Ozcan, A. Perazzo, M. Perl, S. Petrak, B. N. Ratcliff, A. Roodman, A. A. Salnikov, R. H. Schindler, J. Schwiening, G. Simi, A. Snyder, A. Soha, J. Stelzer, D. Su, M. K. Sullivan, J. Va'vra, S. R. Wagner, M. Weaver, A. J. R. Weinstein, W. J. Wisniewski, M. Wittgen, D. H. Wright, A. K. Yarritu, and C. C. Young
Stanford Linear Accelerator Center, Stanford, CA 94309, USA

P. R. Burchat, A. J. Edwards, T. I. Meyer, B. A. Petersen, and C. Roat
Stanford University, Stanford, CA 94305-4060, USA

S. Ahmed, M. S. Alam, J. A. Ernst, M. A. Saeed, M. Saleem, and F. R. Wappler
State University of New York, Albany, NY 12222, USA

W. Bugg, M. Krishnamurthy, and S. M. Spanier
University of Tennessee, Knoxville, TN 37996, USA

R. Eckmann, H. Kim, J. L. Ritchie, A. Satpathy, and R. F. Schwitters
University of Texas at Austin, Austin, TX 78712, USA

J. M. Izen, I. Kitayama, X. C. Lou, and S. Ye
University of Texas at Dallas, Richardson, TX 75083, USA

F. Bianchi, M. Bona, F. Gallo, and D. Gamba
Università di Torino, Dipartimento di Fisica Sperimentale and INFN, I-10125 Torino, Italy

L. Bosisio, C. Cartaro, F. Cossutti, G. Della Ricca, S. Dittongo, S. Grancagnolo, L. Lanceri, P. Poropat,[§] L. Vitale, and G. Vuagnin
Università di Trieste, Dipartimento di Fisica and INFN, I-34127 Trieste, Italy

R. S. Panvini
Vanderbilt University, Nashville, TN 37235, USA

Sw. Banerjee, C. M. Brown, D. Fortin, P. D. Jackson, R. Kowalewski, J. M. Roney, and R. J. Sobie
University of Victoria, Victoria, BC, Canada V8W 3P6

H. R. Band, B. Cheng, S. Dasu, M. Datta, A. M. Eichenbaum, M. Graham, J. J. Hollar, J. R. Johnson, P. E. Kutter, H. Li, R. Liu, A. Mihalyi, A. K. Mohapatra, Y. Pan, R. Prepost, P. Tan, J. H. von Wimmersperg-Toeller, J. Wu, S. L. Wu, and Z. Yu
University of Wisconsin, Madison, WI 53706, USA

M. G. Greene and H. Neal
Yale University, New Haven, CT 06511, USA

The process $e^+e^- \rightarrow \pi^+\pi^-\pi^0\gamma$ has been studied at a center-of-mass energy near the $\Upsilon(4S)$ resonance using a 89.3 fb^{-1} data sample collected with the BABAR detector at the PEP-II collider. From the measured 3π mass spectrum we have obtained the products of branching fractions for the ω and ϕ mesons, $\mathcal{B}(\omega \rightarrow e^+e^-)\mathcal{B}(\omega \rightarrow 3\pi) = (6.70 \pm 0.06 \pm 0.27) \times 10^{-5}$ and $\mathcal{B}(\phi \rightarrow e^+e^-)\mathcal{B}(\phi \rightarrow 3\pi) = (4.30 \pm 0.08 \pm 0.21) \times 10^{-5}$, and evaluated the $e^+e^- \rightarrow \pi^+\pi^-\pi^0$ cross section for the e^+e^- center-of-mass energy range 1.05 to 3.00 GeV. About 900 $e^+e^- \rightarrow J/\psi\gamma \rightarrow \pi^+\pi^-\pi^0\gamma$ events have been selected and the branching fraction $\mathcal{B}(J/\psi \rightarrow \pi^+\pi^-\pi^0) = (2.18 \pm 0.19)\%$ has been measured.

PACS numbers: 13.66.Bc, 14.40.Cs, 13.25.Gv, 13.25.Jx, 13.20.Jf

*Now at Department of Physics, University of Warwick, Coventry,

United Kingdom

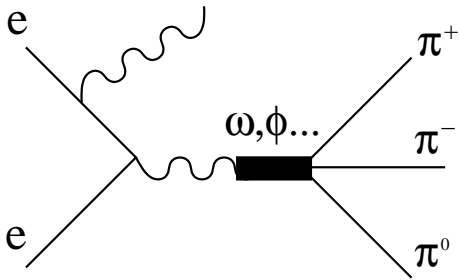


FIG. 1: The diagram for the $e^+e^- \rightarrow \pi^+\pi^-\pi^0\gamma$ process.

I. INTRODUCTION

The analysis of the process $e^+e^- \rightarrow \gamma + \text{hadrons}$, where the photon emission is caused by initial state radiation (ISR), can be used to measure the e^+e^- annihilation cross section into hadrons over a wide range of center-of-mass (c.m.) energy in a single experiment [1–3]. In these events, the invariant mass, $\sqrt{s'}$, of the final state hadronic system corresponds to the “effective” center-of-mass energy after ISR.

This method, currently used both at the KLOE experiment at DAFNE (Frascati) [4] and at the BABAR experiment at the PEP-II B Factory (SLAC), is applied here to study the process $e^+e^- \rightarrow \pi^+\pi^-\pi^0$ at low energies (1 to 3 GeV).

The Born cross section for the $e^+e^- \rightarrow \text{hadrons} + \gamma$ process (Fig. 1) integrated over the momenta of the hadrons is given by

$$\frac{d\sigma(s, x, \theta)}{dx d\cos\theta} = W(s, x, \theta) \sigma_0(s(1-x)), \quad (1)$$

where \sqrt{s} is the e^+e^- center-of-mass energy, $x \equiv 2E_\gamma/\sqrt{s}$, E_γ and θ are the photon energy and polar angle in the c.m. frame, and $s(1-x) = s'$, already mentioned above. Here σ_0 is defined as the Born cross section for $e^+e^- \rightarrow \text{hadrons}$. The so-called radiator function (see, for example, Ref. [3])

$$W(s, x, \theta) = \frac{\alpha}{\pi x} \left(\frac{2 - 2x + x^2}{\sin^2\theta} - \frac{x^2}{2} \right) \quad (2)$$

describes the probability of ISR photon emission for $\theta \gg m_e/\sqrt{s}$. Here α is the fine structure constant and m_e is the electron mass. The ISR photons are emitted predominantly at small angles relative to the initial electron or positron directions; however about 10% of the photons have c.m. polar angles in the range $30^\circ < \theta < 150^\circ$. In

the present analysis, we require that the ISR photon is detected.

The differential cross section for ISR production of a narrow resonance (vector meson V), such as J/ψ , decaying into the final state f can be calculated using [3]

$$\frac{d\sigma(s, \theta)}{d\cos\theta} = \frac{12\pi^2 \Gamma(V \rightarrow e^+e^-) \mathcal{B}(V \rightarrow f)}{m s} W(s, x_0, \theta), \quad (3)$$

where m and $\Gamma(V \rightarrow e^+e^-)$ are the mass and electronic width of the vector meson V , $x_0 = 1 - m^2/s$, and $\mathcal{B}(V \rightarrow f)$ is the branching fraction of V into the final state f . Therefore, the measurement of the number of $J/\psi \rightarrow 3\pi$ decays in $e^+e^- \rightarrow 3\pi\gamma$ determines the product of the electronic width and the branching fraction: $\Gamma(J/\psi \rightarrow e^+e^-) \mathcal{B}(J/\psi \rightarrow 3\pi)$.

The $e^+e^- \rightarrow \pi^+\pi^-\pi^0$ cross section in the energy region $\sqrt{s'} \lesssim 1$ GeV is dominated by the $\omega(782)$ and $\phi(1020)$ mesons¹. This energy region has been studied in many experiments with high statistics and the Particle Data Group (PDG) parameters [5] for ω and ϕ mesons have relatively high precision (2–3% for $\mathcal{B}(V \rightarrow e^+e^-) \mathcal{B}(V \rightarrow 3\pi)$ and about 1% for the total widths).

The energy region above the ϕ was studied in two experiments: SND [6] for energies up to 1.4 GeV with statistical precision about 10% and DM2 [7] for energies in the 1.34–2.40 GeV range with statistical precision about 25%. As pointed out in Ref. [6], there is a significant systematic shift between these two datasets, and the DM2 data need to be scaled by a factor 1.72 ± 0.24 in order to fit with those of SND.

In this energy region, the $e^+e^- \rightarrow 3\pi$ cross section is generally described as the sum of two resonances $\omega'(1420)$ and $\omega''(1650)$. So cross section measurement allows the determination of the ω' and ω'' parameters. Masses, widths, and decay modes for these resonances are not well established. The PDG [5] gives only estimates for these parameters.

The main goal of this analysis is an independent measurement of the $e^+e^- \rightarrow \pi^+\pi^-\pi^0$ cross section in the energy region from 1.05 to 3.00 GeV. The aim is to significantly improve the precision of the cross section for energies above 1.4 GeV. Our data in the $\omega - \phi$ region can be compared with the more precise e^+e^- data in this region and the difference can be used to check our systematic error estimation.

We study J/ψ production in the process $e^+e^- \rightarrow \pi^+\pi^-\pi^0\gamma$, and measure the product $\Gamma(J/\psi \rightarrow e^+e^-) \mathcal{B}(J/\psi \rightarrow 3\pi)$. The branching fraction $\mathcal{B}(J/\psi \rightarrow 3\pi)$ is then determined using the known value of $\Gamma(J/\psi \rightarrow e^+e^-)$ [8]. The decay $J/\psi \rightarrow 3\pi$ has been studied in many experiments [9–15] but only three of them measured the decay rate without any restrictions on the

[†]Also with Università della Basilicata, Potenza, Italy

[‡]Also with IFIC, Instituto de Física Corpuscular, CSIC-Universidad de Valencia, Valencia, Spain

[§]Deceased

¹ Throughout this paper, 2π , 3π , and 4π mean $\pi^+\pi^-$, $\pi^+\pi^-\pi^0$, and $\pi^+\pi^-\pi^0\pi^0$, respectively. We also use the notations ω , ϕ , ω' , and ω'' for $\omega(782)$, $\phi(1020)$, $\omega(1420)$, and $\omega(1650)$.

invariant mass of the two-pion system. Three results for $\mathcal{B}(J/\psi \rightarrow 3\pi)$ are $(1.6 \pm 0.4)\%$ [12], $(1.5 \pm 0.2)\%$ [13], $(1.42 \pm 0.19)\%$ [14]. The average of these measurements is $(1.47 \pm 0.13)\%$. This value is in significant disagreement with more recent result from the BES Collaboration [16]: $(2.10 \pm 0.12)\%$.

II. THE BABAR DETECTOR AND DATA SAMPLES

In this paper a data sample of 89.3 fb^{-1} , collected by the *BABAR* detector [17] at the PEP-II asymmetric-energy storage ring, is analyzed. At PEP-II, 9-GeV electrons collide with 3.1-GeV positrons at a center-of-mass energy of 10.6 GeV ($\Upsilon(4S)$ resonance).

Charged-particle tracking for the *BABAR* detector is provided by a five-layer silicon vertex tracker (SVT) and a 40-layer drift chamber (DCH), operating in a 1.5-T axial magnetic field. The transverse momentum resolution is 0.47% at 1 GeV/c. Energies of photons and electrons are measured with a CsI(Tl) electromagnetic calorimeter (EMC) with a resolution of 3% at 1 GeV. Charged-particle identification is provided by ionization measurements in the SVT and DCH, and by an internally reflecting ring-imaging Cherenkov detector (DIRC). Muons are identified in the solenoid's instrumented flux return, which consists of iron plates interleaved with resistive plate chambers.

Signal and background ISR processes are simulated using Monte Carlo (MC) event generators based on the computer code described in Ref. [18]. The event generator for the $e^+e^- \rightarrow 3\pi\gamma$ reaction uses a model with an intermediate $\rho\pi$ state. The background process $e^+e^- \rightarrow \pi^+\pi^-\pi^0\pi^0\gamma$ is simulated with $\omega\pi^0$ and $a_1(1260)\pi$ intermediate states in the proportion that matches existing experimental data. The extra soft-photon radiation is generated with the use of the structure function method of Ref. [19] and the PHOTOS package [20] for electron and charged hadron bremsstrahlung, respectively. Since the polar-angle distribution of the ISR photon is peaked near 0° and 180° , the events are generated with the restriction on the photon polar angle in the c.m. frame, $20^\circ < \theta < 160^\circ$. We also require that the invariant mass of the hadron system and ISR photon together is greater than $8 \text{ GeV}/c^2$. This second cut restricts the maximum energy of extra photons emitted by the initial particles. The background processes $e^+e^- \rightarrow \pi^+\pi^-\gamma$, $\mu^+\mu^-\gamma$ are generated with the Phokhara program [21], which includes next-to-leading-order QED corrections and simulates the emission of two hard photons at large angle by the initial particles. The background from $e^+e^- \rightarrow q\bar{q}$ and $e^+e^- \rightarrow \tau^+\tau^-$ is simulated with JETSET [22] and KORALB [23] packages, respectively. The interaction of the generated particles with the *BABAR* detector and the detector response are simulated using the GEANT4 [24] package. The simulation takes into account the variation of the detector and accelerator conditions, and in partic-

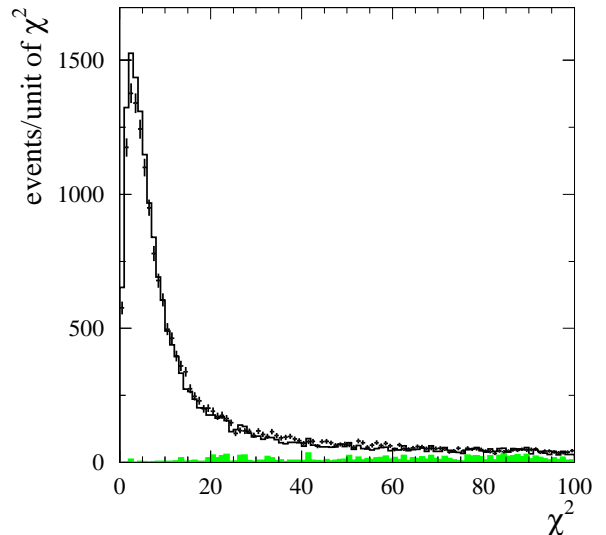


FIG. 2: The χ^2 distributions for data (points with error bars) and simulated (histogram) events from the ω mass region. The shaded histogram shows the distribution for simulated background events.

ular describes the beam-induced background, which leads to the appearance of photons and tracks overlapping on the events of interest.

III. EVENT SELECTION

The initial selection of $e^+e^- \rightarrow \pi^+\pi^-\pi^0\gamma$ candidates requires that all the final particles are detected inside a fiducial volume. (All kinematic variables used in the paper are defined in the laboratory frame unless otherwise stated.) Since a significant fraction of the events contain beam-generated spurious tracks and photons, we select events with two or three tracks and at least three photons that have energies above 100 MeV and polar angles in the range $23^\circ < \theta < 137.5^\circ$ (the corresponding angular range in the c.m. frame is $38^\circ < \theta < 154^\circ$). One of the photons is required to have an energy in the c.m. frame above 3 GeV. Two of the tracks must originate from the interaction point, have a transverse momentum above 100 MeV/c and be in the polar angle region between 23° and 140° . Background events from the process $e^+e^- \rightarrow e^+e^-\gamma$ are suppressed by requiring the ratio of the calorimeter-deposited energy to the track momentum, E_{EMC}/p , to be below 0.9 for the two highest-momentum tracks.

The photon with greatest c.m. energy is assumed to be the ISR photon. The remaining photons are paired to form candidate π^0 s, requiring that their invariant mass must be in the range 0.07 to $0.20 \text{ GeV}/c^2$. A kinematic fit is applied to the selected event, imposing energy and momentum conservation, and constraining the candidate

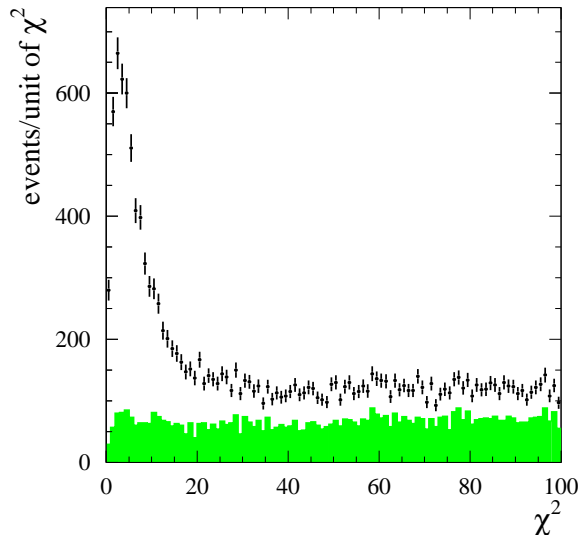


FIG. 3: The χ^2 distributions for data from the mass range $1.05 < M_{3\pi} < 3.00 \text{ GeV}/c^2$. The shaded histogram shows events rejected by background suppression cuts.

π^0 invariant mass. The MC simulation does not accurately reproduce the shape of the resolution function for the photon energy. This leads to a difference in the distributions of the χ^2 of the kinematic fit for data and simulation. To reduce this difference only the measured direction of the ISR photon is used in the fit; its energy is a free fit parameter. In the case of events with three tracks, the fit uses the parameters of the two tracks with opposite charge that have the minimum distance from the interaction point in the azimuthal plane. For events with more than three photons all possible combinations of photons are tested and the one with minimum χ^2 is used. The events with very high χ^2 (> 10000) are considered as not reconstructed.

The χ^2 of the kinematic fit is used to discriminate real $3\pi\gamma$ events from background. Figure 2 shows the χ^2 distribution for events from the 3π mass region near the ω mass ($0.75\text{--}0.82 \text{ GeV}/c^2$), where the contribution of background processes is small. Events with $\chi^2 < 40$ are selected to analyze the 3π mass spectrum. The rest of the sample ($10000 > \chi^2 > 40$) is used to study both background processes and possible selection-efficiency corrections due to data-MC simulation differences in the χ^2 distribution. The χ^2 distribution for masses $1.05 < M_{3\pi} < 3.00 \text{ GeV}/c^2$ (Fig. 3) shows that a significant fraction of events in this mass range correspond to background processes.

The main sources of background are other ISR processes ($e^+e^- \rightarrow \pi^+\pi^-\pi^0\pi^0\gamma$, $\pi^+\pi^-\gamma$, $K^+K^-\pi^0\gamma$, etc.) and e^+e^- annihilation to $q\bar{q}$ and $\tau^+\tau^-$. Additional background suppression cuts are applied to improve the signal-to-background ratio in the mass region of interest.

The ISR events with kaons in the final state ($e^+e^- \rightarrow$

$K^+K^-\pi^0\gamma$, $e^+e^- \rightarrow K^+K^-\gamma$) are suppressed using the kaon identification based on dE/dx measurements in the tracking devices, and the value of the Cherenkov angle and the number of photons measured in the DIRC. The requirement that none of the charged tracks is identified as a kaon rejects about 95% of the kaon-induced background with only 4% loss of $3\pi\gamma$ events.

The radiative events $e^+e^- \rightarrow \pi^+\pi^-\gamma$ and $e^+e^- \rightarrow \mu^+\mu^-\gamma$ with extra photons having $\gamma\gamma$ invariant mass close to that of a π^0 are suppressed by a cut on the π^0 energy. The cut $E_{\pi^0} > 0.4 \text{ GeV}$ rejects 80% of $e^+e^- \rightarrow \pi^+\pi^-\gamma$ and $e^+e^- \rightarrow \mu^+\mu^-\gamma$ events with about 4% loss of $3\pi\gamma$ events.

The process $e^+e^- \rightarrow \pi^+\pi^-\pi^0\pi^0\gamma$ with a soft π^0 is the main source of background for the process under study. Some fraction of $4\pi\gamma$ events reconstructed as $\pi^+\pi^-\pi^0\gamma$ contain a π^0 among extra photons. We select these events by performing a kinematic fit for the $4\pi\gamma$ hypothesis. The requirement $\chi^2_{4\pi\gamma} > 40$ rejects about 40% of $4\pi\gamma$ events and only 2% of $3\pi\gamma$ events.

The main source of background from $e^+e^- \rightarrow \tau^+\tau^-$ is the events in which both τ 's decay into $2\pi\nu$. The hard photon arises from a π^0 decay. Since the $\tau \rightarrow 2\pi\nu$ decay proceeds mainly via $\rho\nu$, such events must have the invariant mass of the most energetic photon and one of the charged pions peaked near the ρ mass. The cut $M_{\pi\gamma} > 1.5 \text{ GeV}/c^2$ almost fully rejects $e^+e^- \rightarrow \tau^+\tau^-$ background and leads to only 0.3% loss of $3\pi\gamma$ events. The remaining $\tau^+\tau^-$ background is estimated to be less than 0.1% of $3\pi\gamma$ events.

Another possible background source is events from e^+e^- annihilation into hadrons containing a very energetic π^0 . A fraction of these events can be seen in the distribution of invariant mass ($M_{\gamma\gamma}^*$) of two photons, one of which is the most energetic in an event. The second photon in the pair is required to have an energy above 100 MeV. Once all possible photon pair combinations are checked, the one with closest invariant mass to the π^0 mass is chosen. The events with $0.10 < M_{\gamma\gamma}^* < 0.17 \text{ GeV}/c^2$ are rejected.

The χ^2 distribution for all rejected events is shown as the shaded histogram in Fig. 3. It is seen from Fig. 3 that we reject more than 60% of background events without significant loss of signal events.

IV. BACKGROUND CALCULATION AND SUBTRACTION

The χ^2 distribution and 3π mass spectrum for data and for simulation of $e^+e^- \rightarrow \pi^+\pi^-\pi^0\gamma$ and background processes after imposing the background suppression cuts are shown in Figs. 4 and 5. The remaining background can be divided into two classes with different χ^2 distributions. The first class includes $e^+e^- \rightarrow K^+K^-\pi^0\gamma$ and $e^+e^- \rightarrow \pi^+\pi^-\pi^0\pi^0$ processes, which have χ^2 distributions peaked at low χ^2 . The second class includes all other background processes. The simulated χ^2 distribu-

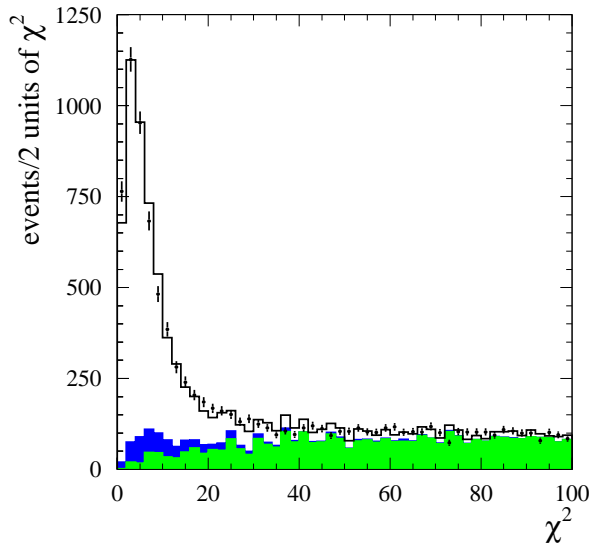


FIG. 4: The χ^2 distribution for events from the mass range $1.05 < M_{3\pi} < 3.00$ GeV/c^2 after background suppression cuts. The points with error bars show the data distribution. The histogram is the sum of simulated distributions for $e^+e^- \rightarrow \pi^+\pi^-\pi^0\gamma$ and background processes. The dark and light shaded histograms show the distributions for $e^+e^- \rightarrow \pi^+\pi^-\pi^0\pi^0$ and other background processes, respectively.

tion for these processes is shown by the lightly shaded histogram in Fig. 4. The background events from the first class must be subtracted bin-by-bin from the $M_{3\pi}$ spectrum.

The mass distribution for kaon events surviving the selection (N_{0K}) can be obtained from the distribution of events with two identified kaons (N_{2K}): $N_{0K}(M_{3\pi}) = N_{2K}(M_{3\pi})R_K$. The coefficient R_K is determined from the simulation, which uses kaon identification efficiency corrections obtained from a pure kaon sample from D^* decays to improve the agreement of data and simulation. The value of R_K is found to be independent of $M_{3\pi}$ and equal to 0.09 ± 0.01 . The total fraction of kaon events in the final event sample is estimated to be 0.4%.

The simulation shows that about 80% of the $e^+e^- \rightarrow q\bar{q}$ events that pass the selection criteria have $\pi^+\pi^-\pi^0\pi^0$ as the final state. In order to cross-check the value of the yield given by JETSET fragmentation for this particular final state, we use the following procedure to extract the mass distribution for $e^+e^- \rightarrow \pi^+\pi^-\pi^0\pi^0$ from experimental data. We select events with two charged particles and four photons with energy more than 0.1 GeV, at least one of them with c.m. energy more than 3 GeV, perform a kinematic fit to the $e^+e^- \rightarrow \pi^+\pi^-\pi^0\pi^0$ hypothesis and require the χ^2 of this fit to be less than 20. The number of selected 4π events is found to be about 15% less than the number expected from JETSET. We also studied various two- and three-particle mass distributions and find that both in data and simulation the $e^+e^- \rightarrow \pi^+\pi^-\pi^0\pi^0$

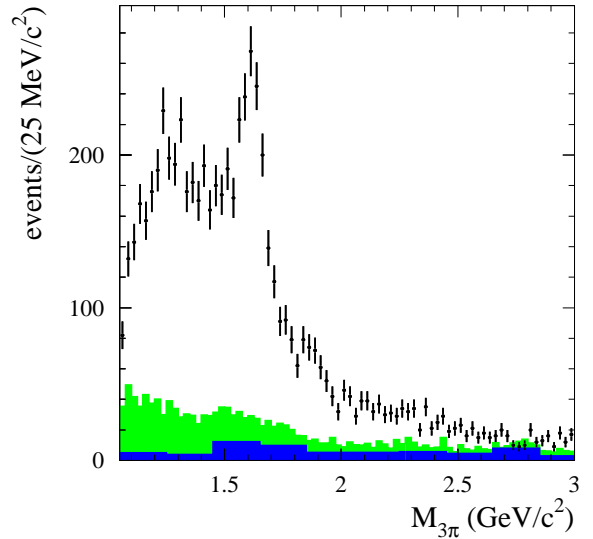


FIG. 5: The 3π mass spectrum for data events with $\chi^2 < 40$. The light blue shaded histogram shows the mass spectrum for calculated background. The dark blue histogram is $e^+e^- \rightarrow \pi^+\pi^-\pi^0\pi^0$ background.

process proceeds via the $\rho\pi\pi$ state. No other intermediate states are seen. To obtain the 3π mass spectrum for $e^+e^- \rightarrow \pi^+\pi^-\pi^0\pi^0$ events reconstructed in the $e^+e^- \rightarrow \pi^+\pi^-\pi^0\gamma$ hypothesis ($(dN/dm)_{3\pi\gamma}$), we multiply the 3π mass spectrum of selected 4π events ($(dN/dm)_{4\pi}^{exp}$) by the ratio of corresponding simulated distributions: $(dN/dm)_{3\pi\gamma}^{MC}/(dN/dm)_{4\pi}^{MC}$. The resulting mass spectrum is shown in Fig. 5 as the dark shaded histogram. The fraction of this background does not exceed 10% in the mass region below 2 GeV/c^2 and rises at higher masses.

The main contribution to the second class of background events comes from the $e^+e^- \rightarrow \pi^+\pi^-\pi^0\pi^0\gamma$ and $e^+e^- \rightarrow \pi^+\pi^-\gamma$ processes. To estimate the accuracy of the MC simulation prediction of the background level for these processes we use events with $\chi^2 > 40$. Fitting distributions of the 3π and $\pi^+\pi^-$ invariant masses for these predominantly background events with a sum of distributions for the signal and background processes, we find scale factors of (1.00 ± 0.25) for $4\pi\gamma$ and (3 ± 1) for $2\pi\gamma$. Figures 6 and 7 show the fitted $M_{3\pi}$ and $M_{\pi^+\pi^-}$ distributions for events with $100 < \chi^2 < 500$. The quoted errors in the scale factors are much larger than the statistical errors from the fits and originate from systematic effects. For $4\pi\gamma$ events the error is determined by the dependence of the scale factor value on χ^2 . For $2\pi\gamma$ events we observe a significant difference in the shape of the 3π mass distribution between data and simulation and the 30% systematic error has been assigned to cover the uncertainty on the mass spectrum.

We attribute this difference and the large value of the $2\pi\gamma$ scale factor to the inaccuracy of the simulation of

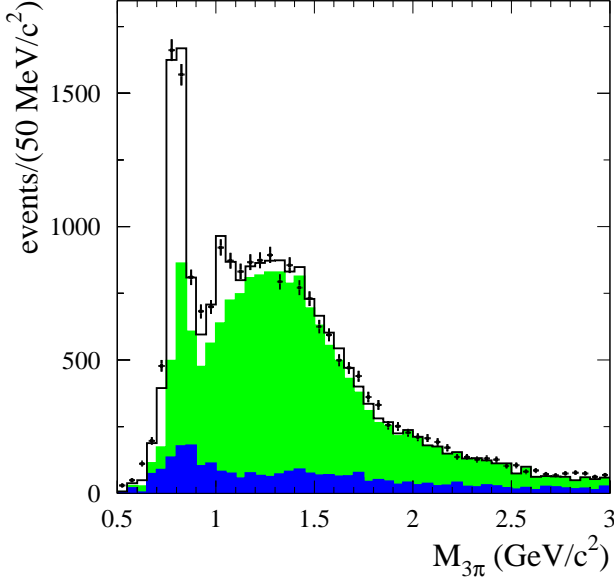


FIG. 6: The $M_{3\pi}$ spectrum for events with $100 < \chi^2 < 500$ and $E_{\pi^0} > 1$ GeV. The points with error bars are data. The histogram is the sum of spectra for simulated events of $e^+e^- \rightarrow \pi^+\pi^-\pi^0\gamma$ and background processes. The lightly shaded histogram is the sum of all background processes. The difference between the dark and lightly shaded histograms shows the $e^+e^- \rightarrow \pi^+\pi^-\pi^0\pi^0\gamma$ contribution.

π -meson nuclear interactions in the EMC. This leads to a difference between data and MC simulation in the multiplicities of spurious photons arising from the nuclear interaction, and their energy and angular distributions. This conclusion is supported by the fact that the scale factor for $e^+e^- \rightarrow \mu^+\mu^-\gamma$ background events is found to be close to unity. The $e^+e^- \rightarrow \mu^+\mu^-\gamma$ events were selected using muon identification criteria based on EMC and IFR information. The level of $e^+e^- \rightarrow \mu^+\mu^-\gamma$ background is found to be (5–15)% of the $2\pi\gamma$ background.

Another source of the second class of background, non- 4π $e^+e^- \rightarrow q\bar{q}$, $q = u, d, s, c$, does not exceed 10% of the total level of background for masses up to $2.5 \text{ GeV}/c^2$. Since the accuracy of the JETSET prediction for the $e^+e^- \rightarrow \pi^+\pi^-\pi^0\pi^0$ process is at the 15% level, we conservatively assume that the predictions for non- 4π backgrounds are accurate to better than 50%.

The production of a π^0 or a photon with c.m. energy more than 3 GeV in $B\bar{B}$ events is kinematically forbidden. We therefore do not expect any background from B decays.

The calculated level of background is about 0.6% in the ω mass region and 1.4% in the ϕ mass region. The 3π mass spectrum above the ϕ for data and background events is shown in Fig. 5. The level of background is 15% at $1.5 \text{ GeV}/c^2$ and 50% at $3 \text{ GeV}/c^2$. The systematic uncertainty on the background level is about 25%

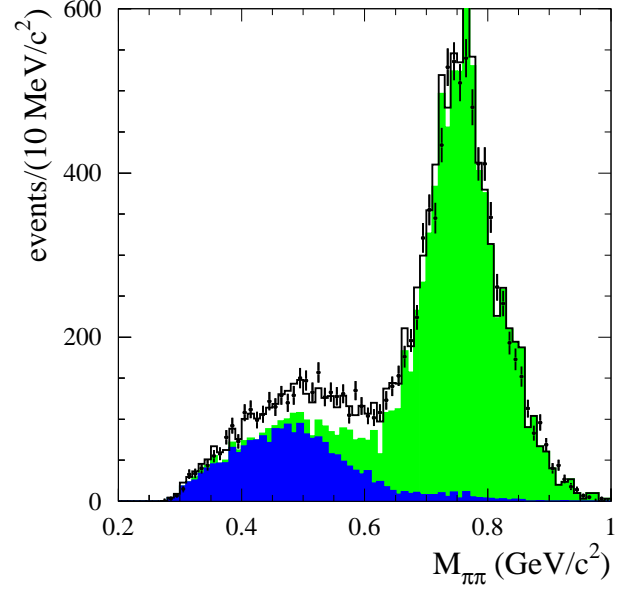


FIG. 7: $\pi^+\pi^-$ invariant mass spectrum for events with $100 < \chi^2 < 500$ and $0.85 < M_{3\pi} < 1.05 \text{ GeV}/c^2$. The points with error bars are data. The histogram is the sum of spectra for simulated events of $e^+e^- \rightarrow \pi^+\pi^-\pi^0\gamma$ and background processes. The lightly shaded histogram is the sum of all background processes. The difference between the dark and lightly shaded histogram shows the $e^+e^- \rightarrow \pi^+\pi^-\pi^0\gamma$ contribution.

below $2 \text{ GeV}/c^2$. For higher masses the fractional uncertainty grows due to an uncertainty in the $q\bar{q}$ background calculation, a model dependence in the simulation of $e^+e^- \rightarrow 2\pi\gamma$ and $e^+e^- \rightarrow 4\pi\gamma$ (the processes $e^+e^- \rightarrow 2\pi$ and $e^+e^- \rightarrow 4\pi$ have not been measured for e^+e^- c.m. energies above 2 GeV), and the possible contribution of unaccounted ISR processes ($e^+e^- \rightarrow \pi^+\pi^- 3\pi^0\gamma$, $\pi^+\pi^- 4\pi^0\gamma$, etc.).

We therefore use two different methods for background subtraction. For masses below $1.05 \text{ GeV}/c^2$, where the level of background is low, we subtract the calculated background. For higher masses we use the procedure of statistical subtraction based on the difference in χ^2 distributions of signal and background events.

The statistical subtraction procedure is as follows. For each mass bin we find the numbers of events with $\chi^2 \leq 20$ (N_1) and $20 < \chi^2 < 40$ (N_2) and calculate the number of signal and background events with $\chi^2 < 40$ as

$$N_s = \frac{(1 - \beta)N_1 - \beta N_2}{\alpha - \beta}, \quad (4)$$

$$N_{bkg} = \frac{\alpha N_2 - (1 - \alpha)N_1}{\alpha - \beta}, \quad (5)$$

where $\alpha, \beta = N_1/(N_1 + N_2)$ for pure signal and background events, respectively. N_1 and N_2 in Eq. (4–5) do

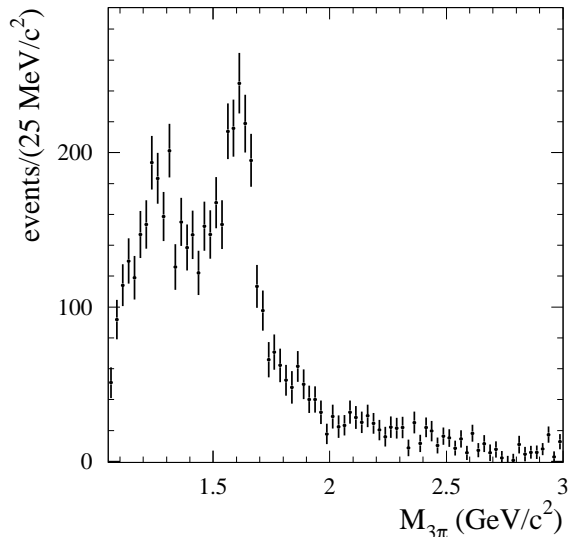


FIG. 8: The 3π mass spectrum for data obtained after the statistical background-subtraction procedure.

not contain events $e^+e^- \rightarrow K^+K^-\pi^0\gamma$ and $e^+e^- \rightarrow \pi^+\pi^-\pi^0\pi^0$ processes, which are subtracted from both mass distributions bin-by-bin.

The coefficient β is determined from the simulation. Its values for the main background processes in four mass regions are listed in Table I. It is seen that there is no significant dependence of β on the mass and that the three main background process have consistent values of β . We therefore use the average value $\beta = 0.33 \pm 0.02 \pm 0.05$. The variation of the β values for different processes was used as an estimate of the systematic error.

The values of α at the ϕ and J/ψ masses are extracted from data. In the ϕ mass region we determine the ratio $N_1/(N_1 + N_2)$ for pure signal events from the experimental χ^2 distribution with subtracted background. The value of α at the J/ψ mass is measured by another method. The numbers of J/ψ events for different χ^2 cuts are determined using a mass-sideband subtraction method (see Sec. VIII). The resulting values of α are $0.879 \pm 0.006 \pm 0.005$ at the ϕ mass and 0.882 ± 0.014 at the J/ψ mass. The systematic error on α at the ϕ mass is estimated by varying the calculated background level by $\pm 25\%$. For the mass range 1.05-3.00 GeV/c^2 we use a linear interpolation between the ϕ and J/ψ values of α .

The 3π mass spectrum obtained after this statistical background subtraction is shown in Fig. 8. The 3π mass distribution for the background events obtained using Eq. (5) is shown in Fig. 9 and compared with the MC simulation. The simulation describes well both the shape of the background spectrum and the total number of events up to at least 2.5 GeV/c^2 . The shapes of the signal and background distributions are quite different.

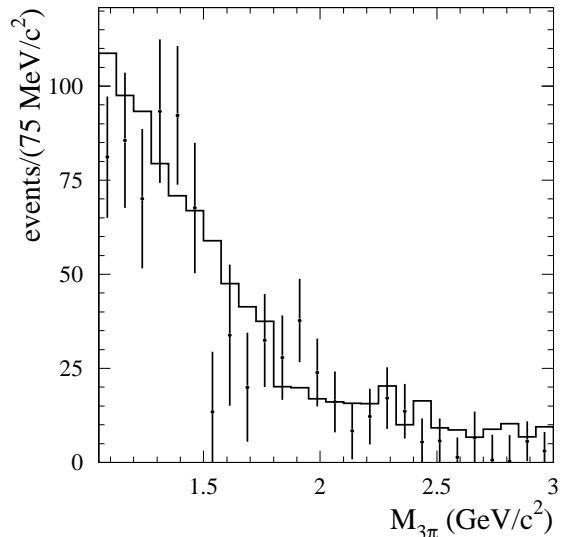


FIG. 9: The 3π mass spectrum for background events obtained from the statistical background-subtraction procedure (points with error bars). The histogram shows the background mass distribution expected from MC simulation.

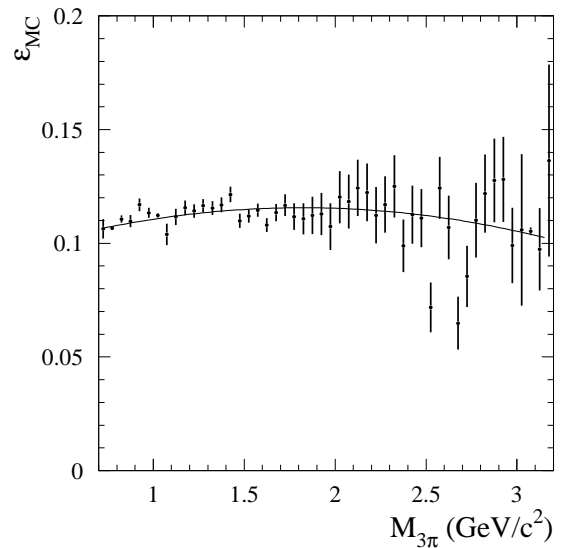


FIG. 10: The 3π -mass dependence of the detection efficiency obtained from MC simulation. The line is the fit to a second-order polynomial.

V. DETECTION EFFICIENCY

To first approximation the detection efficiency is determined from MC simulation as the ratio of the true 3π mass distribution computed after and before applying the selection criteria. The detection efficiency calculated in this way, shown in Fig. 10, is fit to a second-order polynomial. This efficiency (ϵ_{MC}) must be corrected to account

TABLE I: The values of $\beta = N(\chi^2 < 20)/N(\chi^2 < 40)$ calculated for different background processes in four mass regions. w is the relative contribution of the process to the total background. On the average, each value of β is weighted by the corresponding value of w .

process	$1.05 < M_{3\pi} \leq 1.40$		$1.4 < M_{3\pi} \leq 2.0$		$2.0 < M_{3\pi} \leq 2.5$		$2.5 < M_{3\pi} < 3.0$		$1.05 < M_{3\pi} < 3.00$	
	$w(\%)$	β	$w(\%)$	β	$w(\%)$	β	$w(\%)$	β	$w(\%)$	β
$\pi^+\pi^-\pi^0\pi^0\gamma$	68	0.30 ± 0.02	70	0.33 ± 0.02	67	0.34 ± 0.03	35	0.36 ± 0.05	66	0.32 ± 0.01
$\pi^+\pi^-\gamma, \mu^+\mu^-\gamma$	28	0.33 ± 0.10	20	0.35 ± 0.14	27	0.54 ± 0.20	42	0.29 ± 0.19	26	0.36 ± 0.07
$q\bar{q}, \tau^+\tau^-$	4	0.39 ± 0.12	10	0.40 ± 0.08	6	0.50 ± 0.20	23	0.30 ± 0.11	8	0.38 ± 0.06
Average		0.32 ± 0.03		0.34 ± 0.03		0.40 ± 0.07		0.32 ± 0.09		0.33 ± 0.02

for data-MC simulation differences in detector response:

$$\varepsilon = \varepsilon_{MC}/\Pi(1 + \delta_i), \quad (6)$$

where δ_i are efficiency corrections, for each of several effects. These corrections are discussed below and summarized in Table II. They are determined at the ω , ϕ , and J/ψ masses, where the relative level of background is small, and a linear interpolation between their values is used for the mass ranges between the ω , ϕ , and J/ψ .

Our preliminary selection contains a cut on the energy deposited by charged pions in the calorimeter ($E_{EMC}/p < 0.9$), which is not simulated accurately. The momentum dependence of the probability for a pion to have $E_{EMC}/p > 0.9$ is found using events for the process $e^+e^- \rightarrow \pi^+\pi^-\pi^+\pi^-\gamma$ selected without cuts on energy deposition in the calorimeter. The value of the efficiency correction is about 3%.

The efficiency correction for the background suppression cuts is determined from ratios of the number of events selected with and without the background suppression cuts, in data and MC simulation. We use events with $\chi^2 < 20$ from mass ranges near the ω , ϕ , and J/ψ . In data the fraction of signal events rejected by these cuts varies from 13% in the ω and ϕ mass region to 20% at J/ψ . This dependence is reproduced by the simulation. The efficiency correction is about 3% for all masses.

To determine the efficiency correction due to the $\chi^2 < 40$ cut, we fit the 3π mass spectrum in the $\phi - \omega$ mass range for events with $\chi^2 < 40$, $40 < \chi^2 < 500$, and $500 < \chi^2 < 1000$ to a sum of simulated signal and background distributions with free simulated factors. The fit for events with $40 < \chi^2 < 500$ is shown in Fig. 11. The data-MC simulation discrepancy is estimated by the double ratio

$$g(500) = \frac{N_{sig}(40 < \chi^2 < 500)/N_{MC}(40 < \chi^2 < 500)}{N_{sig}(\chi^2 < 40)/N_{MC}(\chi^2 < 40)},$$

where N_{MC} is the number of simulated events and N_{sig} is the number of signal events in data obtained from the fit to $M_{3\pi}$ in the corresponding χ^2 interval. We obtain $g(500) = 1.30 \pm 0.04$ and, for the $500 < \chi^2 < 1000$ interval, $g(1000) = 1.29 \pm 0.17$. For higher χ^2 the relative signal level is too small to determine its value. From the measured values of $g(500)$ and $g(1000)$ and simulated χ^2 distributions, we calculate the efficiency correction for the $\omega - \phi$ mass region to be $(9 \pm 3)\%$. The quoted error

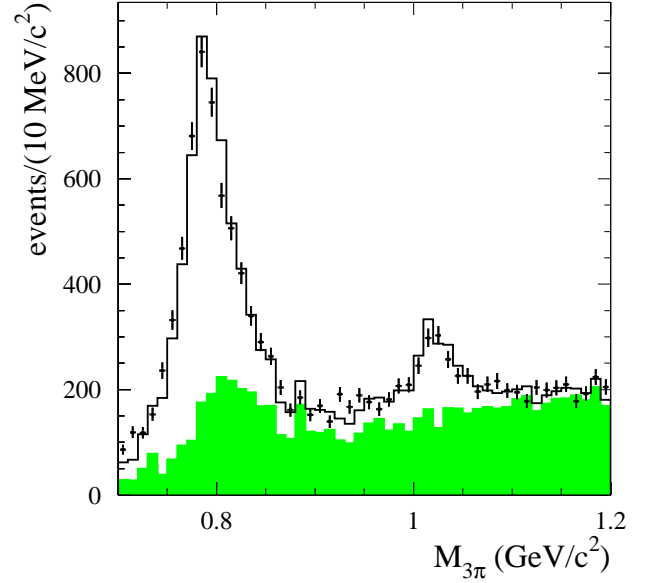


FIG. 11: The 3π mass spectrum for events with $40 < \chi^2 < 500$. Points with error bars show the data distribution. The solid line shows the sum of the distributions for simulated $e^+e^- \rightarrow \pi^+\pi^-\pi^0\gamma$ and background processes. The shaded histogram shows the distribution for background processes.

includes uncertainties due to errors on the g values and the uncertainty due to events with $\chi^2 > 1000$. For these events the g value found for the $500 < \chi^2 < 1000$ interval is used. In the J/ψ mass region we use a mass-sideband subtraction method to determine the numbers of signal events with $\chi^2 < 40$ and $40 < \chi^2 < 500$ in data and MC simulation. For higher χ^2 we do not see a J/ψ signal due to large background levels. The obtained value of $g(500) = 1.12 \pm 0.20$ agrees with the result for the $\phi - \omega$ mass region. Using this number for all χ^2 we find the efficiency correction at the J/ψ mass to be $(4 \pm 6)\%$.

The other possible source of data-MC simulation difference is π^0 losses due to the merging of electromagnetic showers of the two photons from the π^0 decay or the loss of one of the decay photons. To study the π^0 losses we perform a kinematic fit for data and simulated events with the $e^+e^- \rightarrow \pi^+\pi^-\pi^0\gamma$ hypothesis using the measured parameters for only the two charged tracks and

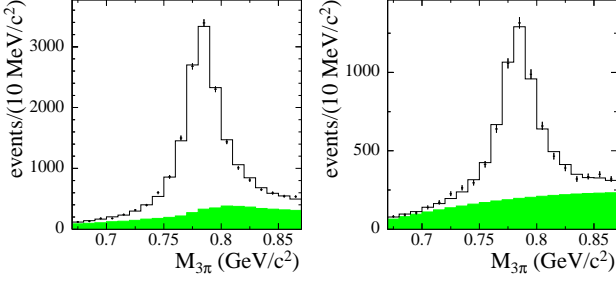


FIG. 12: The 3π mass distribution for events selected without using the photons from the π^0 decay, that are reconstructed (left) and not reconstructed (right) with our standard kinematic fit procedure. Points with error bars show the data distribution. The solid line is a fit result. The shaded histogram is the fitted background contribution.

the ISR photon. The π^0 energy and angles are determined as a result of the fit. To suppress background we use a very tight cut on the χ^2 of the fit and require that the total energy of all photons in the event, excluding the ISR photon candidate, is greater than 80% of the π^0 energy found in the fit. The high level of remaining background does not allow determination of the efficiency correction for masses above the ω . Therefore, we restrict our study to the ω -mass region. The 3π mass spectra for selected events reconstructed ($\chi^2 < 10000$) and not reconstructed with our standard kinematic fit procedure are shown in Fig. 12. The fraction of events that are not reconstructed is about 30%. In most of these events one of the photons from the π^0 decay is outside the polar angle range used in our standard selection. The mass spectra are fit to a sum of distributions for signal and background events. The signal distribution is extracted from the simulation. The background spectrum is a sum of the simulated distribution for $e^+e^- \rightarrow \pi^+\pi^-\pi^0\pi^0\gamma$ events and a second order polynomial with free coefficients. The efficiency correction due to π^0 losses is determined to be $\delta = \epsilon_{MC}/\epsilon_{exp} - 1 = -(1.9 \pm 0.9)\%$. Here ϵ is the fraction of events with a π^0 reconstructed with the constrained fit discussed above that, after the standard kinematic fit procedure, pass the $\chi^2 < 10000$ selection. To calculate the correction for higher masses we must take into account the dependence of the shape of the π^0 energy spectrum on the 3π mass. At the ω mass we determine the correction as a function of π^0 energy and convolve this function with the π^0 energy spectra at the ϕ and J/ψ masses. The calculated corrections are $-(1.7 \pm 0.9)\%$ and $-(1.5 \pm 0.8)\%$ for ϕ and J/ψ masses, respectively.

We also studied the quality of the simulation of trigger and background filters used in event reconstruction. The corresponding efficiency corrections are listed in Table II. We use the overlap of the samples of events passing either different filters or trigger criteria and the partial independence of these filters or triggers to measure their efficiency.

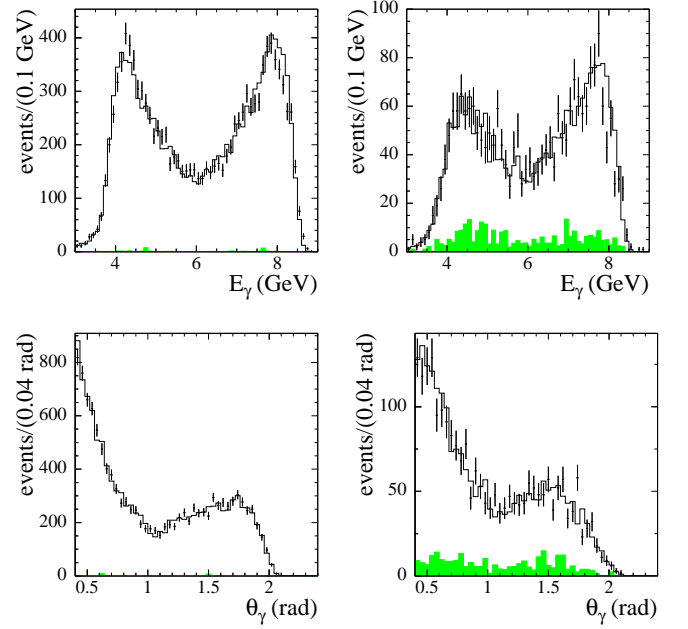


FIG. 13: Distributions of the ISR photon energy (1st row) and polar angle (2nd row) for data (points with error bars) and simulation (solid line) events with $\chi^2 < 20$. The left and right columns correspond to the mass regions $0.75 < M_{3\pi} < 0.82$ GeV/ c^2 and $1.40 < M_{3\pi} < 1.80$ GeV/ c^2 , respectively. Shaded histograms show the calculated background contributions.

The data-MC simulation difference in track losses is studied by comparing the ratios of $e^+e^- \rightarrow \pi^+\pi^-\pi^+\pi^-\gamma$ events with three and four tracks in data and MC simulation. The difference in data and simulated probabilities to lose one of four tracks is found to be $(3.6 \pm 2.0)\%$. For the case of two tracks we estimate the corresponding efficiency correction to be $(1.8 \pm 1.8)\%$. We increase the systematic error to account for the possible dependence of the correction on track multiplicity and track momenta.

The data-MC simulation difference in the probability of photon conversion in the detector material before the DCH is studied using $e^+e^- \rightarrow \gamma\gamma$ events and is found to be $-(0.4 \pm 0.2)\%$. We estimate that the total correction for conversion of one of the three photons in an event is $-(1.0 \pm 0.6)\%$. The fact that part of this correction is already included in the correction for π^0 loss is accounted for in the determination of this value.

The event generator for the $e^+e^- \rightarrow 3\pi\gamma$ reaction uses a model with an intermediate $\rho\pi$ state. This model has been checked for the $\omega - \phi$ mass region in several high statistics e^+e^- experiments [25–27]. Small deviations from the $\rho\pi$ model found in the ϕ meson decays [27] are negligible at our statistical level. Figures 13, 14, and 15 demonstrate a good agreement between the data and simulated distributions over both the kinematical and dynamical (di-pion invariant masses) parameters for the ω mass region.

In the mass region above the ϕ the intermediate state

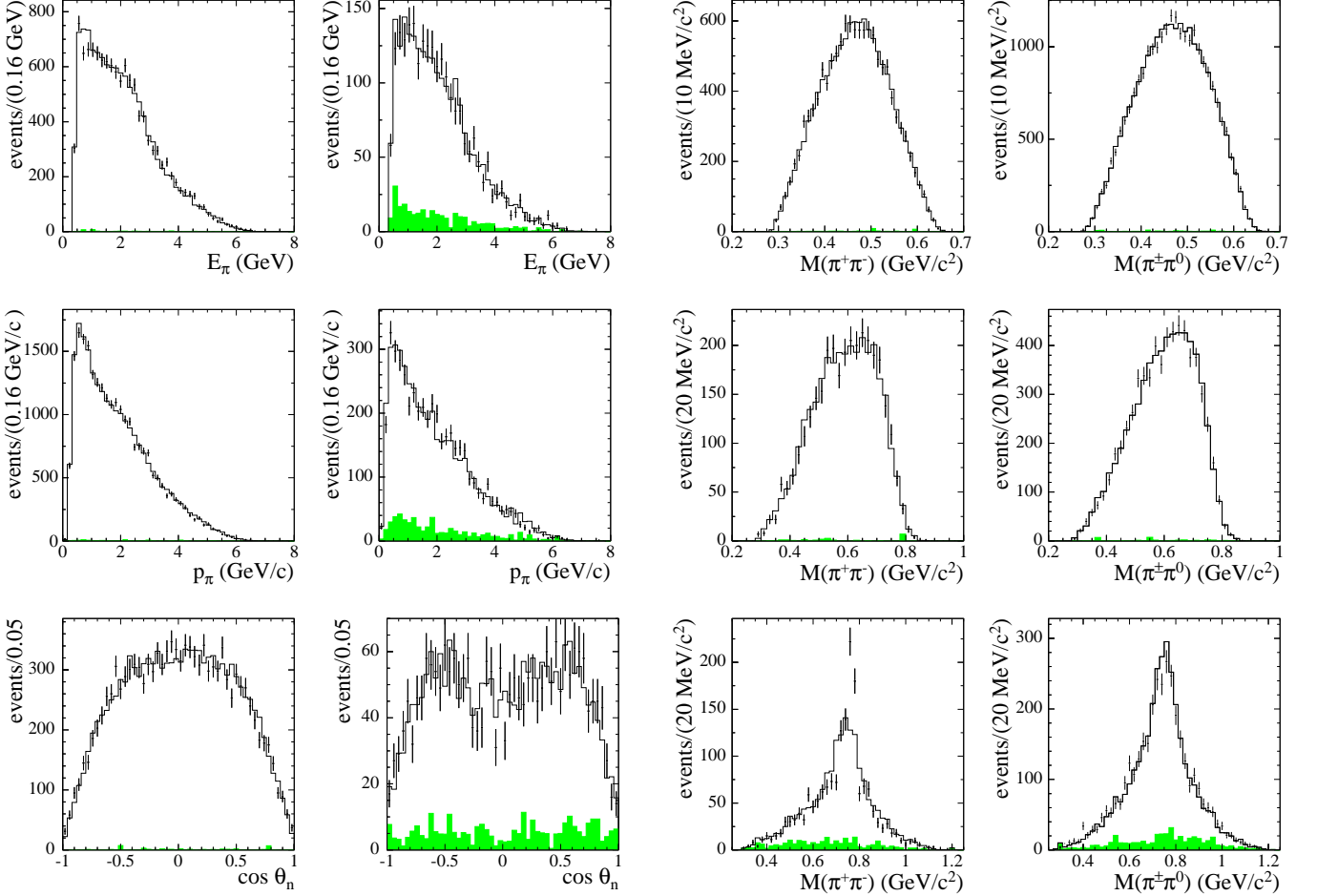


FIG. 14: Distributions of π^0 energy (1st row), charged pion momentum (2nd row), and angle between the normal to the 3π plane in the three-pion rest frame and the direction of the 3π system in the laboratory frame (3rd row) for data (points with error bars) and simulation (solid line) events with $\chi^2 < 20$. The left and right columns correspond to the mass regions $0.75 < M_{3\pi} < 0.82 \text{ GeV}/c^2$ and $1.40 < M_{3\pi} < 1.80 \text{ GeV}/c^2$, respectively. Shaded histograms show the calculated background contributions.

$\omega\pi$ becomes noticeable. This additional mechanism was studied at the SND experiment [6] for the energy region up to 1.4 GeV. It was established that the contribution of the $\omega\pi$ intermediate state to the total cross section of $e^+e^- \rightarrow 3\pi$ process does not exceed 10%.

The distributions of different kinematic parameters for the mass region from 1.4 to 1.8 GeV/c^2 are shown in Figs. 13 and 14. For these parameters the data distributions agree with the simulated ones. In the $\pi^+\pi^-$ mass spectra (Fig. 15) for data, a narrow peak near the ω mass is seen. The fraction of events in this peak is about 10% for $1.1 < M_{3\pi} < 1.4 \text{ GeV}/c^2$ and 6% for $1.4 < M_{3\pi} < 1.8 \text{ GeV}/c^2$ in agreement with measurements of SND [6]. We calculate the detection efficiency for simulated events with $0.77 < M_{\pi^+\pi^-} < 0.80 \text{ GeV}/c^2$

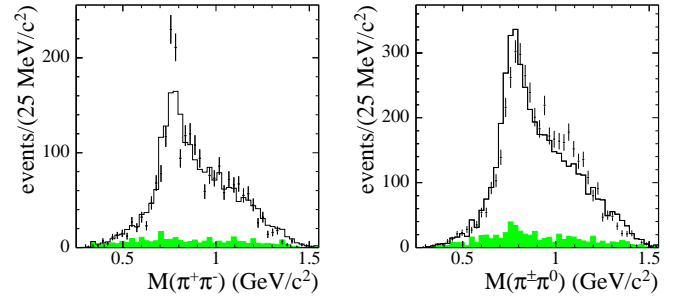


FIG. 15: Distributions of $\pi^+\pi^-$ (left column) and $\pi^\pm\pi^0$ (right column) invariant masses for data (points with error bars) and simulation (solid line) for events with $\chi^2 < 20$. The rows correspond to the mass regions: $0.75 < M_{3\pi} < 0.82 \text{ GeV}/c^2$ (1st row), $1.00 < M_{3\pi} < 1.04 \text{ GeV}/c^2$ (2nd row), $1.10 < M_{3\pi} < 1.40 \text{ GeV}/c^2$ (3rd row), and $1.40 < M_{3\pi} < 1.80 \text{ GeV}/c^2$ (4th row). Shaded histograms show the calculated background contributions.

and find its difference with detection efficiency for the full $M_{\pi^+\pi^-}$ mass range to be $(1.6 \pm 3.9)\%$.

There are also noticeable deviations from the MC simulation in the distribution of the $\pi^\pm\pi^0$ invariant mass for the mass region $1.4 < M_{3\pi} < 1.8 \text{ GeV}/c^2$ (Fig. 15), which are manifest in the shift of the visible ρ -meson mass po-

sition and a bump at a mass above 1 GeV/ c^2 . A possible explanation of this difference is the appearance at higher masses of the $\omega'' \rightarrow \rho'\pi$ transition, which interferes with the $\rho\pi$ amplitude. We study the dependence of the detection efficiency on $\pi^+\pi^0$ mass and find it to be constant in the mass range $0.65 < M_{\pi^+\pi^0} < 1.25$ GeV/ c^2 . We conclude that the use of the $\rho\pi$ model for the simulation of $e^+e^- \rightarrow 3\pi\gamma$ does not lead to any significant errors in the determination of the detection efficiency.

Efficiency corrections δ_i are summarized in Table II. The total efficiency corrections δ calculated from $1 + \delta = \Pi(1 + \delta_i)$ are listed in the last row of the table. The correction is 14% near the ω and ϕ , and 11% at the J/ψ mass.

VI. FIT TO THE $\pi^+\pi^-\pi^0$ INVARIANT MASS DISTRIBUTION

In order to determine the peak cross sections for e^+e^- annihilation into ω and ϕ mesons and the resonance parameters of excited ω states, we fit the background-subtracted 3π invariant-mass spectrum. The mass spectrum is described by the following function:

$$\frac{dN}{dm} = \sigma_{3\pi}(m) \frac{dL}{dm} R \varepsilon, \quad (7)$$

where $\sigma_{3\pi}(m)$ is the Born cross section for $e^+e^- \rightarrow 3\pi$, dL/dm is the so-called ISR differential luminosity, ε is the detection efficiency as a function of mass, and R is a radiative correction factor accounting for the Born mass spectrum distortion due to emission of several photons by the initial electron and positron. The ISR luminosity is calculated using the total integrated luminosity L and the probability density function for ISR photon emission (Eq. (2)):

$$\frac{dL}{dm} = \frac{\alpha}{\pi x} \left((2 - 2x + x^2) \log \frac{1+C}{1-C} - x^2 C \right) \frac{2m}{s} L. \quad (8)$$

Here $x = 1 - m^2/s$, \sqrt{s} is the e^+e^- c.m. energy, $C = \cos \theta_0$, and θ_0 determines the range of polar angles in the c.m. frame: $\theta_0 < \theta_\gamma < 180^\circ - \theta_0$ for the ISR photon. In our case θ_0 is equal to 20° , since we determine the detector efficiency using the simulation with $20^\circ < \theta_\gamma < 160^\circ$.

The Born cross section for $e^+e^- \rightarrow 3\pi$ can be written as the sum of the contributions of four resonances:

$$\sigma_{3\pi}(m) = \frac{12\pi}{m^3} F_{\rho\pi}(m) \left| \sum_{V=\omega,\phi,\omega',\omega''} \frac{\Gamma_V m_V^{3/2} \sqrt{\mathcal{B}(V \rightarrow e^+e^-) \mathcal{B}(V \rightarrow 3\pi)}}{D_V(m)} \frac{e^{i\phi_V}}{\sqrt{F_{\rho\pi}(m_V)}} \right|^2, \quad (9)$$

where m_V and Γ_V are the mass and width of the resonance V , ϕ_V is its phase, $\mathcal{B}(V \rightarrow e^+e^-)$ and $\mathcal{B}(V \rightarrow 3\pi)$ are the branching fractions of V into e^+e^- and 3π ,

$$D_V(m) = m_V^2 - m^2 - im\Gamma_V(m), \quad \Gamma_V(m) = \sum_f \Gamma_f(m).$$

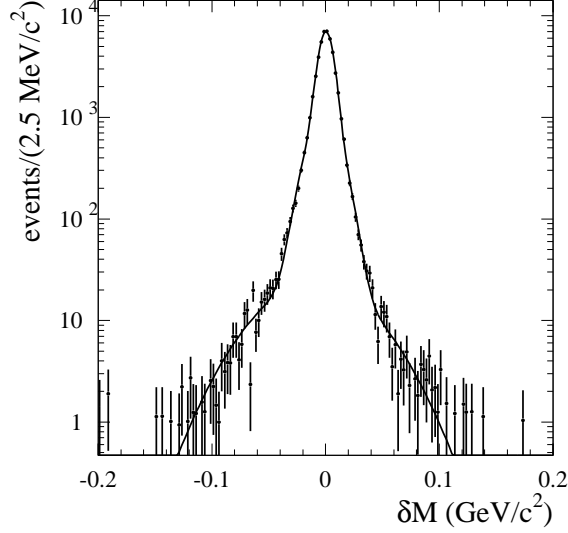
Here $\Gamma_f(m)$ is the mass-dependent partial width of the resonance decay into the final state f , and $\Gamma_f(m_V) = \Gamma_V \mathcal{B}(V \rightarrow f)$. The mass-dependent width for the ω and ϕ mesons has been calculated taking into account all significant decay modes. The corresponding formulae can be found, for example, in Ref. [25]. We assume that $V \rightarrow 3\pi$ decay proceeds via the $\rho\pi$ intermediate state, and $F_{\rho\pi}(m)$ is the 3π phase space volume calculated under this hypothesis. The formula for $F_{\rho\pi}$ calculation can be found in Ref. [25].

The radiative correction factor was determined using Monte Carlo simulation (at the generator level, with no detector simulation). The 3π mass spectrum was generated both using only the pure Born amplitude of the $e^+e^- \rightarrow \pi^+\pi^-\pi^0\gamma$ process and using a model

with higher-order radiative corrections included with the structure function method. With the cut on the invariant mass of the $3\pi\gamma$ system, $M_{3\pi\gamma} > 8$ GeV/ c^2 , used in our simulation, no significant difference is found between these two spectra. Therefore the radiative correction factor is evaluated as the ratio of the total cross section with $M_{3\pi\gamma} > 8$ GeV/ c^2 to the Born cross section and is found to be close to unity, $R = 0.9994$. The theoretical uncertainty in the radiative correction calculation with the structure function method does not exceed 1% [19]. The radiative correction factor does not include the corrections due to leptonic and hadronic vacuum polarization. Here we follow the generally accepted practice [28] of including the vacuum polarization correction in the resonance electronic width. The probability density function (PDF) for the 3π mass spectrum as expressed in Eq. (7) needs to be convolved with the detector resolution function in order to fully characterize the experimental mass distribution found in the data. The detector resolution function is obtained using MC simulation of the detector response. Figure 16 shows the distribution of the difference between measured and true 3π mass for sim-

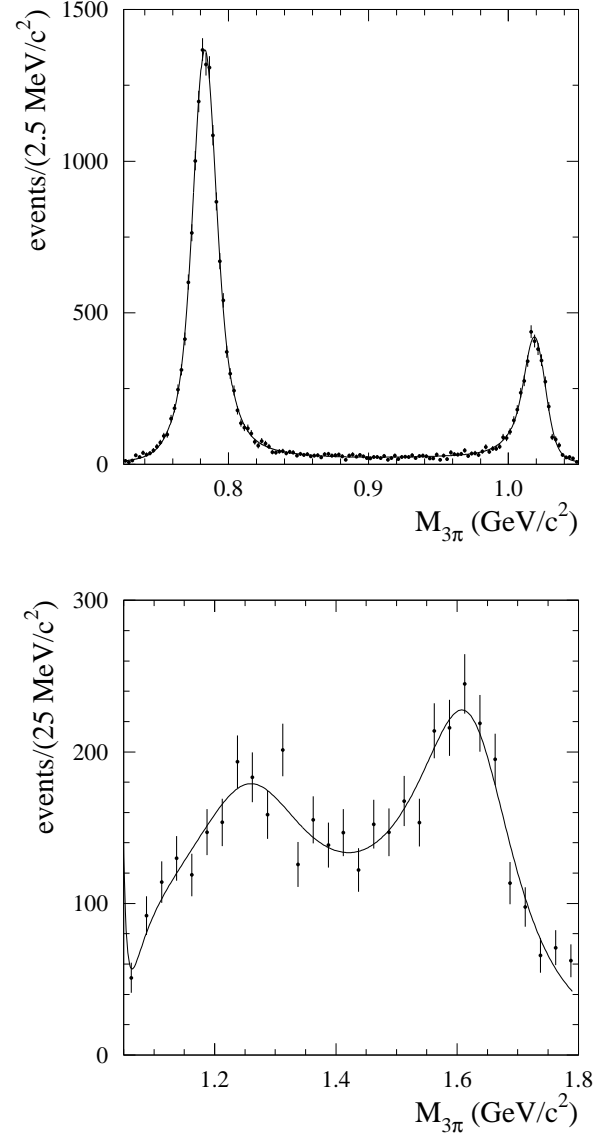
TABLE II: The values of different efficiency corrections δ_i for ω , ϕ , and J/ψ mass regions.

effect	$\delta_i(m_\omega),\%$	$\delta_i(m_\phi),\%$	$\delta_i(m_{J/\psi}),\%$
$E_{EMC}/p < 0.9$ cuts	$+2.9 \pm 0.3$	$+2.9 \pm 0.3$	$+2.5 \pm 0.3$
background rejection cuts	$+3.0 \pm 0.4$	$+2.4 \pm 0.7$	$+2.9 \pm 1.9$
$\chi^2 < 40$ cut	$+9 \pm 3$	$+9 \pm 3$	$+4 \pm 6$
π^0 loss	-1.9 ± 0.9	-1.7 ± 0.9	-1.5 ± 0.8
trigger and filters	$+0.0 \pm 0.4$	$+0.1 \pm 1.0$	$+2.2 \pm 2.0$
track loss	$+1.8 \pm 1.8$	$+1.8 \pm 1.8$	$+1.8 \pm 1.8$
photon conversion	-1.0 ± 0.6	-1.0 ± 0.6	-1.0 ± 0.6
total	$+14 \pm 4$	$+14 \pm 4$	$+11 \pm 7$

FIG. 16: The distribution of the difference between measured and true 3π mass for simulated events with $\chi^2 < 40$ from the mass region near the ω . The curve is a fit to a triple-Gaussian function.

ulated events with $\chi^2 < 40$ in the mass region near the ω . For each 3π mass region, the distribution is fit with a triple-Gaussian function. The resolution depends on the 3π mass and is about 6, 7, and 9 MeV/c^2 at the ω , ϕ and J/ψ masses, respectively. The determination of the resolution function is performed in the ω , ϕ and J/ψ mass regions, where the available Monte Carlo simulation statistics are high enough. For the mass region between the ω and ϕ we use a linear interpolation. Since no narrow peaks are present in the mass region between the ϕ and the J/ψ , it is not critical to know a very detailed resolution function, and therefore an average resolution function is used over the mass range between 1.05 and 3.00 GeV .

A binned maximum likelihood fit is used to fit the 3π mass spectrum in data. The bin width is chosen to be $2.5 \text{ MeV}/c^2$ for the $\omega - \phi$ mass range and $25 \text{ MeV}/c^2$ for masses above the ϕ . The free parameters in the fit are the products of the branching fractions

FIG. 17: The background-subtracted 3π mass spectrum for masses between 0.70 and 1.05 MeV/c^2 (upper plot) and for masses from 1.05 to 1.80 MeV/c^2 (lower plot). The curves are the result of the fit described in the text.

$\mathcal{B}(V \rightarrow e^+e^-)\mathcal{B}(V \rightarrow 3\pi)$, the masses m_V for all four resonances ($V = \omega, \phi, \omega', \omega''$), and the widths for ω' and ω'' . The width of the ω meson is fixed at the value of $(8.68 \pm 0.13) \text{ MeV}/c^2$ obtained recently in the CMD2 [29] and SND [25] experiments. The width of the ϕ meson is fixed at the PDG value. The relative phase between the ω and ϕ amplitudes, $\phi_\phi = (163 \pm 7)^\circ$, is taken from Ref. [25]. The phases of ω, ω' , and ω'' are fixed at values of $0^\circ, 180^\circ$, and 0° [30]. Our fitting function does not take into account the contribution of the $e^+e^- \rightarrow \omega\pi\gamma \rightarrow 3\pi\gamma$ process which proceeds via excited ρ states. In Ref. [6] it is shown that this mechanism does not change significantly the parameters for the ω' and ω'' resonances. The fitted mass region is restricted to masses below 1.8 GeV. To be described properly, data in the higher mass range would require a more complicated function, which would take into account both the resonant and the non-resonant 3π production. There are no reliable models available in the literature, and therefore our results on the parameters of the ω' and ω'' states, obtained in this fit, should only be considered a first approximation.

In order to account for a possible resolution difference between data and simulation, the resolution function determined from simulation is modified by adding or subtracting quadratically an additional σ_G to all sigmas of the triple-Gaussian function. Technically, a squared sigma σ_G^2 is used as a free parameter (with negative values allowed). Two σ_G^2 parameters are used, one for ω and another for ϕ and higher masses.

The fit result is shown along with the data in Fig. 17. The resulting parameters obtained from the fit ($\chi^2/\text{dof} = 146/148$) are the following:

$$\begin{aligned} \mathcal{B}(\omega \rightarrow e^+e^-)\mathcal{B}(\omega \rightarrow 3\pi) &= (6.70 \pm 0.06 \pm 0.27) \times 10^{-5}, \\ m_\omega - m_\omega^{\text{PDG}} &= -(0.2 \pm 0.1) \text{ MeV}/c^2, \\ \sigma_{G\omega}^2 &= (0.9 \pm 1.6) \text{ MeV}^2/c^4, \\ \mathcal{B}(\phi \rightarrow e^+e^-)\mathcal{B}(\phi \rightarrow 3\pi) &= (4.30 \pm 0.08 \pm 0.21) \times 10^{-5}, \\ m_\phi - m_\phi^{\text{PDG}} &= -(0.6 \pm 0.2) \text{ MeV}/c^2, \\ \sigma_{G\phi}^2 &= -(3.2 \pm 2.6) \text{ MeV}^2/c^4, \\ \mathcal{B}(\omega' \rightarrow e^+e^-)\mathcal{B}(\omega' \rightarrow 3\pi) &= (0.82 \pm 0.05 \pm 0.06) \times 10^{-6}, \\ M_{\omega'} &= (1350 \pm 20 \pm 20) \text{ MeV}/c^2, \\ \Gamma_{\omega'} &= (450 \pm 70 \pm 70) \text{ MeV}/c^2, \\ \mathcal{B}(\omega'' \rightarrow e^+e^-)\mathcal{B}(\omega'' \rightarrow 3\pi) &= (1.3 \pm 0.1 \pm 0.1) \times 10^{-6}, \\ M_{\omega''} &= (1660 \pm 10 \pm 2) \text{ MeV}/c^2, \\ \Gamma_{\omega''} &= (230 \pm 30 \pm 20) \text{ MeV}/c^2. \end{aligned}$$

The quoted errors correspond to the statistical and systematic uncertainties, respectively. The systematic error for $\mathcal{B}(V \rightarrow e^+e^-)\mathcal{B}(V \rightarrow 3\pi)$ includes a statistical error from simulation, the error on the efficiency correction (Table II), 1.2% uncertainty in the luminosity, 1% theoretical uncertainty on the radiative correction, a background subtraction uncertainty (0.4% at ω and 0.6% at ϕ), and an uncertainty arising from errors on $\Gamma_\omega, \Gamma_\phi$, and ϕ_ϕ (1% at ω and 2.8% at ϕ). The systematic errors on the masses and widths of the ω' and ω'' mesons are due

to the background-subtraction uncertainty and the errors on $\Gamma_\omega, \Gamma_\phi$, and ϕ_ϕ .

The fitted values $\mathcal{B}(V \rightarrow e^+e^-)\mathcal{B}(V \rightarrow 3\pi)$ for the ω and ϕ mesons are in reasonable agreement with the corresponding world average values [5], $\mathcal{B}(\omega \rightarrow e^+e^-)\mathcal{B}(\omega \rightarrow 3\pi) = (6.35 \pm 0.10) \times 10^{-5}$ and $\mathcal{B}(\phi \rightarrow e^+e^-)\mathcal{B}(\phi \rightarrow 3\pi) = (4.52 \pm 0.19) \times 10^{-5}$. The observed peak positions of both the ω and ϕ are shifted to lower masses relative to their PDG values. The shifts are about $(0.3-0.6) \times 10^{-3}$ of the mass values. The fitted values of σ_G^2 parameters have large statistical uncertainties, and lead to a change in the simulated resolution of (2-3)%.

The fitted masses and widths of the ω' and ω'' mesons can be compared with the estimates of these parameters by the PDG [5]: $M_{\omega'} = 1400 - 1450 \text{ MeV}/c^2$, $\Gamma_{\omega'} = 180 - 250 \text{ MeV}/c^2$, $M_{\omega''} = 1670 \pm 30 \text{ MeV}/c^2$, $\Gamma_{\omega''} = 315 \pm 35 \text{ MeV}/c^2$. The PDG data are based on small data samples for $e^+e^- \rightarrow \omega', \omega'' \rightarrow 3\pi$, $\omega\pi\pi$ [6, 7, 31], $p\bar{p} \rightarrow \omega'\pi^0 \rightarrow \omega\pi^0\pi^0\pi^0$ [32], and $\pi^-p \rightarrow \omega''n \rightarrow \omega\eta n$ [33] reactions. We present a new measurement of the ω' and ω'' parameters based on a significantly larger data sample for the $e^+e^- \rightarrow \omega', \omega'' \rightarrow 3\pi$ reaction. From the measured values of $\mathcal{B}(V \rightarrow e^+e^-)\mathcal{B}(V \rightarrow 3\pi)$, the electronic widths of ω' and ω'' can be estimated. Assuming that $\mathcal{B}(\omega' \rightarrow 3\pi) \approx 1$ and $\mathcal{B}(\omega'' \rightarrow 3\pi) \approx 0.5$ we derive that $\Gamma(\omega' \rightarrow e^+e^-) \approx 370 \text{ eV}$ and $\Gamma(\omega'' \rightarrow e^+e^-) \approx 570 \text{ eV}$. The large values of these widths, comparable with $\Gamma(\omega \rightarrow e^+e^-) \approx 600 \text{ eV}$, are in disagreement with expectations of the quark model, which predicts at least one order of magnitude lower values for the electronic widths for the excited meson states (see, for example, Ref. [34]).

VII. MEASUREMENT OF THE $e^+e^- \rightarrow \pi^+\pi^-\pi^0$ CROSS SECTION

The cross section for $e^+e^- \rightarrow \pi^+\pi^-\pi^0$, in the energy ($\sqrt{s'}$) range between 1.05 and 3.00 GeV, is calculated from the 3π mass spectrum using

$$\sigma_{3\pi}(m) = \frac{(dN/dm)_{\text{corr}}}{\varepsilon R dL/dm}, \quad (10)$$

where $m \equiv \sqrt{s'}$ is the 3π invariant mass, and $(dN/dm)_{\text{corr}}$ is the mass spectrum corrected for resolution effects.

The resolution-corrected mass spectrum is obtained by first subtracting the events with an actual 3π invariant mass outside the 1.05-3.00 GeV/ c^2 region (tails of the ϕ and J/ψ mass distribution). The number of ϕ -meson events with measured mass above 1.05 GeV/ c^2 is estimated from simulation. We subtract 10 ± 5 events from the first mass bin (1.05-1.075 GeV/ c^2). The number of J/ψ events contributing to the mass region under study is found to be 1 ± 1 . Second, the detector resolution is deconvolved by using a migration matrix A that gives the probability that an event with true mass in bin j is

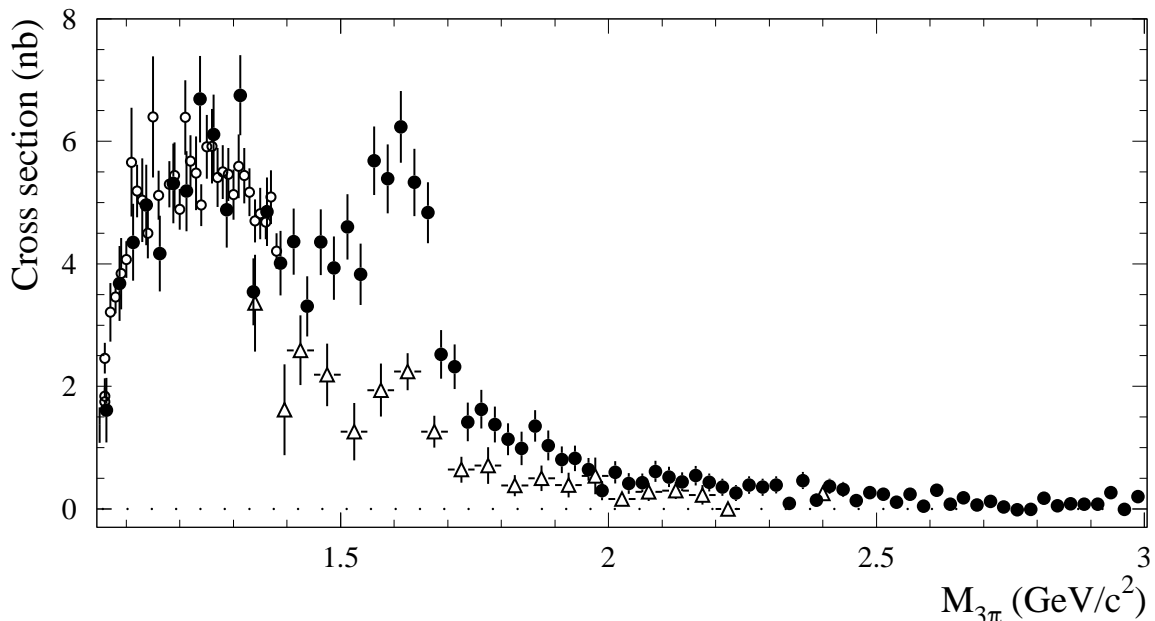


FIG. 18: The $e^+e^- \rightarrow \pi^+\pi^-\pi^0$ cross section measured in this work (filled circles), by SND (open circles), and DM2 (open triangles).

actually reconstructed in bin i :

$$\left(\frac{dN}{dm}\right)_i^{rec} = \sum_j A_{ij} \left(\frac{dN}{dm}\right)_j^{true}. \quad (11)$$

The inverse of this migration matrix (A_{ij}^{-1}) is then applied to the measured spectrum. In our case where the spectrum has no narrow structures and the smearing is small, we can neglect the mass dependence of the resolution and use the average resolution function to build the migration matrix. This allows a determination of the inverse matrix that is robust against statistical fluctuations. The resolution function is obtained from simulation and takes into account our background subtraction procedure. In practice, the only elements of the migration matrix that are significantly different from zero are the diagonal elements, which are around 0.84, and the elements next to the diagonal, which are around 0.08. The resolution correction procedure changes insignificantly the shape of the mass distribution but leads to an increase in the errors (by $\approx 20\%$) and their correlation. The number of events in each bin changes by no more than half its statistical uncertainty. In particular, near 3π mass of 1.6 GeV this change is less than 3%. The number of events for each mass bin is listed in Table III. The quoted errors correspond to the statistical (including the contribution of the background subtraction for the $e^+e^- \rightarrow K^+K^-\pi^0\gamma$ and $e^+e^- \rightarrow \pi^+\pi^-\pi^0\pi^0$ processes) and systematic (due to the α and β parameters) uncertainties.

Table III also contains the values of the detection effi-

ciency and the ISR differential luminosity calculated according to Eq. (8). The errors on the detection efficiency include the uncertainties on the efficiency correction and the statistical errors from the simulation.

The calculated cross section is shown in Fig. 18 and listed in Table III. The quoted errors are statistical and systematic. The latter includes the systematic error contributions from the number of events, and uncertainties in the detection efficiencies and in the calculation of the radiative correction. Note that the systematic errors for different mass bins are fully correlated.

Most of experiments at low energy measure so-called “dressed” cross sections (see, for example, Ref. [6]), which include the vacuum polarization corrections. Since our radiative correction factor R does not take into account vacuum polarization we also measure the “dressed” cross section. A comparison of our measurements with other e^+e^- data is shown in Fig. 18. Our values are in good agreement with SND measurements, but significantly exceed DM2 results.

VIII. MEASUREMENT OF THE $J/\psi \rightarrow 3\pi$ BRANCHING FRACTION

The 3π mass spectrum for selected events in the J/ψ mass region is shown in Fig. 19. The small width of the J/ψ resonance leads to negligible peaking background. For example, $e^+e^- \rightarrow J/\psi\gamma \rightarrow K^+K^-\pi^0\gamma$ events reconstructed under the $3\pi\gamma$ hypothesis have a 3π invariant mass in the range 2.8 to 3.0 GeV/ c^2 . Since the nonreso-

TABLE III: e^+e^- c.m. energy ($\sqrt{s'}$), number of selected events after 3π -mass-resolution correction (N_{corr}), detection efficiency (ε), differential ISR luminosity (L), and measured cross section (σ) for $e^+e^- \rightarrow \pi^+\pi^-\pi^0$. All values are calculated for 25 MeV bin size. The quoted errors are statistical and systematic.

$\sqrt{s'}$ (GeV)	N_{corr}	ε (%)	L (nb $^{-1}$)	σ (nb)	$\sqrt{s'}$ (GeV)	N_{corr}	ε (%)	L (nb $^{-1}$)	σ (nb)
1.0625	40 \pm 13 \pm 3	9.8 \pm 0.4	254	1.61 \pm 0.53 \pm 0.13	2.0375	22 \pm 9 \pm 2	10.2 \pm 0.5	511	0.41 \pm 0.17 \pm 0.04
1.0875	94 \pm 16 \pm 4	9.8 \pm 0.4	260	3.68 \pm 0.61 \pm 0.21	2.0625	23 \pm 8 \pm 1	10.2 \pm 0.5	518	0.43 \pm 0.15 \pm 0.02
1.1125	114 \pm 16 \pm 3	9.8 \pm 0.4	266	4.35 \pm 0.63 \pm 0.21	2.0875	33 \pm 9 \pm 1	10.2 \pm 0.5	525	0.61 \pm 0.17 \pm 0.04
1.1375	133 \pm 18 \pm 4	9.9 \pm 0.4	272	4.96 \pm 0.66 \pm 0.25	2.1125	28 \pm 9 \pm 1	10.2 \pm 0.5	532	0.52 \pm 0.16 \pm 0.03
1.1625	115 \pm 17 \pm 4	9.9 \pm 0.4	278	4.17 \pm 0.62 \pm 0.22	2.1375	24 \pm 8 \pm 1	10.2 \pm 0.5	539	0.44 \pm 0.15 \pm 0.03
1.1875	150 \pm 18 \pm 4	9.9 \pm 0.4	285	5.31 \pm 0.65 \pm 0.25	2.1625	30 \pm 9 \pm 1	10.2 \pm 0.5	547	0.54 \pm 0.16 \pm 0.03
1.2125	150 \pm 19 \pm 4	9.9 \pm 0.4	291	5.19 \pm 0.65 \pm 0.26	2.1875	24 \pm 8 \pm 1	10.2 \pm 0.5	554	0.43 \pm 0.15 \pm 0.03
1.2375	198 \pm 21 \pm 5	9.9 \pm 0.4	297	6.69 \pm 0.71 \pm 0.31	2.2125	20 \pm 8 \pm 1	10.2 \pm 0.5	561	0.36 \pm 0.14 \pm 0.02
1.2625	185 \pm 20 \pm 4	10.0 \pm 0.4	304	6.11 \pm 0.65 \pm 0.27	2.2375	15 \pm 8 \pm 1	10.2 \pm 0.5	569	0.26 \pm 0.13 \pm 0.02
1.2875	151 \pm 19 \pm 5	10.0 \pm 0.4	310	4.88 \pm 0.62 \pm 0.25	2.2625	23 \pm 8 \pm 1	10.2 \pm 0.5	576	0.39 \pm 0.14 \pm 0.03
1.3125	214 \pm 21 \pm 4	10.0 \pm 0.4	316	6.75 \pm 0.65 \pm 0.31	2.2875	21 \pm 8 \pm 1	10.2 \pm 0.5	584	0.36 \pm 0.14 \pm 0.02
1.3375	115 \pm 18 \pm 6	10.0 \pm 0.4	323	3.54 \pm 0.55 \pm 0.23	2.3125	23 \pm 8 \pm 1	10.2 \pm 0.5	591	0.39 \pm 0.14 \pm 0.03
1.3625	160 \pm 19 \pm 4	10.0 \pm 0.4	329	4.85 \pm 0.56 \pm 0.24	2.3375	5 \pm 7 \pm 1	10.1 \pm 0.5	599	0.09 \pm 0.11 \pm 0.01
1.3875	136 \pm 18 \pm 4	10.1 \pm 0.4	335	4.01 \pm 0.53 \pm 0.21	2.3625	28 \pm 9 \pm 1	10.1 \pm 0.6	606	0.46 \pm 0.14 \pm 0.03
1.4125	150 \pm 19 \pm 5	10.1 \pm 0.4	342	4.36 \pm 0.54 \pm 0.24	2.3875	9 \pm 7 \pm 1	10.1 \pm 0.6	614	0.15 \pm 0.11 \pm 0.01
1.4375	116 \pm 17 \pm 5	10.1 \pm 0.4	348	3.31 \pm 0.49 \pm 0.20	2.4125	23 \pm 8 \pm 1	10.1 \pm 0.6	621	0.37 \pm 0.12 \pm 0.02
1.4625	156 \pm 19 \pm 4	10.1 \pm 0.4	355	4.36 \pm 0.54 \pm 0.21	2.4375	20 \pm 8 \pm 1	10.1 \pm 0.6	629	0.32 \pm 0.12 \pm 0.02
1.4875	144 \pm 19 \pm 3	10.1 \pm 0.4	361	3.93 \pm 0.52 \pm 0.20	2.4625	9 \pm 6 \pm 1	10.1 \pm 0.6	637	0.14 \pm 0.10 \pm 0.01
1.5125	172 \pm 20 \pm 4	10.1 \pm 0.4	368	4.60 \pm 0.53 \pm 0.22	2.4875	17 \pm 7 \pm 1	10.0 \pm 0.6	645	0.26 \pm 0.11 \pm 0.02
1.5375	146 \pm 19 \pm 3	10.2 \pm 0.4	374	3.83 \pm 0.50 \pm 0.19	2.5125	16 \pm 7 \pm 1	10.0 \pm 0.6	653	0.24 \pm 0.11 \pm 0.02
1.5625	220 \pm 22 \pm 5	10.2 \pm 0.4	381	5.69 \pm 0.56 \pm 0.28	2.5375	7 \pm 6 \pm 1	10.0 \pm 0.6	660	0.11 \pm 0.09 \pm 0.01
1.5875	213 \pm 22 \pm 5	10.2 \pm 0.4	387	5.39 \pm 0.56 \pm 0.27	2.5625	16 \pm 7 \pm 1	10.0 \pm 0.6	668	0.24 \pm 0.10 \pm 0.02
1.6125	250 \pm 23 \pm 5	10.2 \pm 0.5	394	6.24 \pm 0.58 \pm 0.31	2.5875	3 \pm 6 \pm 1	10.0 \pm 0.6	676	0.05 \pm 0.08 \pm 0.01
1.6375	218 \pm 22 \pm 5	10.2 \pm 0.5	401	5.33 \pm 0.55 \pm 0.27	2.6125	21 \pm 7 \pm 1	9.9 \pm 0.6	684	0.30 \pm 0.10 \pm 0.02
1.6625	201 \pm 21 \pm 4	10.2 \pm 0.5	407	4.84 \pm 0.50 \pm 0.24	2.6375	6 \pm 6 \pm 1	9.9 \pm 0.6	693	0.08 \pm 0.08 \pm 0.01
1.6875	107 \pm 17 \pm 3	10.2 \pm 0.5	414	2.52 \pm 0.40 \pm 0.14	2.6625	13 \pm 7 \pm 1	9.9 \pm 0.6	701	0.18 \pm 0.10 \pm 0.01
1.7125	100 \pm 16 \pm 2	10.2 \pm 0.5	421	2.32 \pm 0.36 \pm 0.12	2.6875	5 \pm 7 \pm 1	9.9 \pm 0.6	709	0.07 \pm 0.09 \pm 0.01
1.7375	62 \pm 14 \pm 2	10.2 \pm 0.5	427	1.42 \pm 0.31 \pm 0.08	2.7125	9 \pm 6 \pm 1	9.8 \pm 0.6	717	0.12 \pm 0.09 \pm 0.01
1.7625	72 \pm 14 \pm 2	10.2 \pm 0.5	434	1.63 \pm 0.31 \pm 0.09	2.7375	2 \pm 5 \pm 1	9.8 \pm 0.6	725	0.03 \pm 0.08 \pm 0.01
1.7875	62 \pm 13 \pm 2	10.2 \pm 0.5	441	1.38 \pm 0.29 \pm 0.07	2.7625	-1 \pm 5 \pm 1	9.8 \pm 0.6	734	-0.01 \pm 0.07 \pm 0.01
1.8125	52 \pm 12 \pm 1	10.2 \pm 0.5	448	1.14 \pm 0.26 \pm 0.06	2.7875	0 \pm 5 \pm 1	9.8 \pm 0.6	742	0.00 \pm 0.07 \pm 0.01
1.8375	46 \pm 13 \pm 3	10.2 \pm 0.5	455	0.99 \pm 0.27 \pm 0.07	2.8125	13 \pm 7 \pm 1	9.7 \pm 0.6	751	0.17 \pm 0.09 \pm 0.01
1.8625	64 \pm 12 \pm 2	10.3 \pm 0.5	462	1.35 \pm 0.26 \pm 0.07	2.8375	4 \pm 6 \pm 1	9.7 \pm 0.6	759	0.05 \pm 0.08 \pm 0.01
1.8875	50 \pm 12 \pm 2	10.3 \pm 0.5	468	1.04 \pm 0.24 \pm 0.07	2.8625	6 \pm 5 \pm 1	9.7 \pm 0.6	768	0.08 \pm 0.07 \pm 0.01
1.9125	39 \pm 11 \pm 2	10.3 \pm 0.5	475	0.80 \pm 0.22 \pm 0.06	2.8875	6 \pm 5 \pm 1	9.6 \pm 0.6	776	0.08 \pm 0.07 \pm 0.01
1.9375	41 \pm 10 \pm 1	10.3 \pm 0.5	482	0.83 \pm 0.21 \pm 0.05	2.9125	6 \pm 5 \pm 1	9.6 \pm 0.6	785	0.08 \pm 0.07 \pm 0.01
1.9625	32 \pm 9 \pm 1	10.3 \pm 0.5	489	0.64 \pm 0.19 \pm 0.04	2.9375	20 \pm 7 \pm 1	9.6 \pm 0.6	794	0.26 \pm 0.09 \pm 0.02
1.9875	15 \pm 8 \pm 1	10.3 \pm 0.5	496	0.30 \pm 0.16 \pm 0.03	2.9625	-1 \pm 5 \pm 1	9.5 \pm 0.6	802	-0.01 \pm 0.06 \pm 0.01
2.0125	31 \pm 9 \pm 1	10.2 \pm 0.5	503	0.60 \pm 0.18 \pm 0.04	2.9875	16 \pm 6 \pm 1	9.5 \pm 0.6	811	0.20 \pm 0.08 \pm 0.01

TABLE IV: N_{signal} and N_{side} are the numbers of selected events in the signal region ($3.0 \leq M_{3\pi} \leq 3.2$ GeV/ c^2) and the sidebands ($2.9 \leq M_{3\pi} < 3.0$ and $3.2 \leq M_{3\pi} < 3.3$ GeV/ c^2), respectively.

	N_{signal}	N_{side}	$N_{signal} - N_{side}$
data	1023	103	920 \pm 34
MC	1825	13	1812 \pm 43

nant background is small and well described by a linear function, a mass-sideband subtraction method is used to determine the number of J/ψ events. Table VIII shows the numbers of data and simulated $3\pi\gamma$ events in the

signal region ($3.0 < M_{3\pi} < 3.2$ GeV/ c^2) and in the sidebands ($2.9 < M_{3\pi} < 3.0$ GeV/ c^2 and $3.2 < M_{3\pi} < 3.3$ GeV/ c^2).

The Monte Carlo simulation of the number of events in the signal and sideband regions is used to estimate a detection efficiency of $\varepsilon_{MC} = 0.101 \pm 0.002$. The data-MC simulation differences discussed earlier are used to correct the former efficiency value by $(11 \pm 7)\%$.

The simulation uses the $\rho\pi$ model of $J/\psi \rightarrow 3\pi$ decay. In order to check the model dependence of the detection efficiency, the Dalitz plot for events in the J/ψ peak (Fig. 20) is analyzed. It is seen that the main mechanism for $J/\psi \rightarrow 3\pi$ decay is $\rho\pi$. There is, however, a difference between the data and simulated plots (an absence

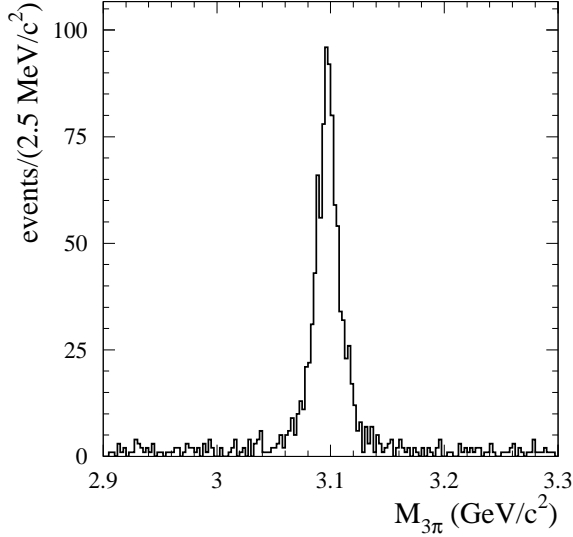


FIG. 19: 3π mass spectrum for selected $e^+e^- \rightarrow J/\psi\gamma \rightarrow \pi^+\pi^-\pi^0\gamma$ events.

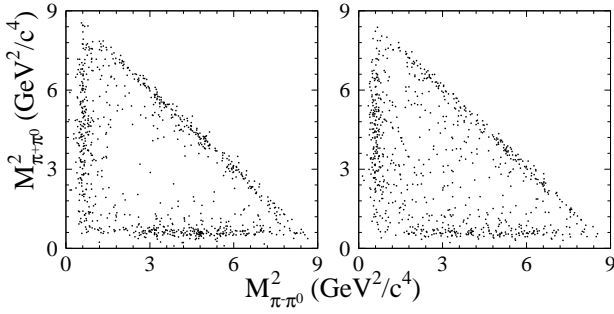


FIG. 20: The Dalitz plot for $J/\psi \rightarrow 3\pi$ candidates in data (left) and simulation (right).

of events in the center of the Dalitz plot for data), which can be a manifestation of negative interference with the contribution of intermediate states other than the $\rho\pi$ [35]. The influence of this difference on the detection efficiency is studied by excluding events located in the center of the Dalitz plot in the simulated sample, and recomputing the detection efficiency. The result is a $(1.1 \pm 0.6)\%$ rise in efficiency. This correction is included with a systematic error of 1.1% in the final calculation of the detection efficiency, which is determined to be 0.092 ± 0.006 .

The cross section for $e^+e^- \rightarrow J/\psi\gamma \rightarrow \pi^+\pi^-\pi^0\gamma$ for $20^\circ < \theta_\gamma < 160^\circ$ is calculated as

$$\sigma(20^\circ < \theta_\gamma < 160^\circ) = \frac{N_{\text{signal}} - N_{\text{side}}}{\varepsilon R L} = (112 \pm 4 \pm 8) \text{ fb.}$$

The radiative-correction factor $R = \sigma/\sigma_{\text{Born}}$, of $1.005 \pm 0.002 \pm 0.010$ used here, is obtained from a MC simulation at the generator level (no detector simulation). The total integrated luminosity for the data sample is $(89.3 \pm 1.1) \text{ fb}^{-1}$. From the measured cross section and Eq. (3), the

following product can be determined:

$$\begin{aligned} \Gamma(J/\psi \rightarrow e^+e^-) \mathcal{B}(J/\psi \rightarrow 3\pi) \\ = (0.122 \pm 0.005 \pm 0.008) \text{ keV.} \end{aligned}$$

The systematic error includes the uncertainties on the detection efficiency, the integrated luminosity, and the radiative correction.

The most precise measurement of the electronic width was made in the analysis of $e^+e^- \rightarrow J/\psi\gamma \rightarrow \mu^+\mu^-\gamma$ by *BABAR* [8]: $\Gamma(J/\psi \rightarrow e^+e^-) = (5.61 \pm 0.20) \text{ keV}$. Using the latter measurement, the $J/\psi \rightarrow 3\pi$ branching fraction is calculated to be

$$\mathcal{B}(J/\psi \rightarrow 3\pi) = (2.18 \pm 0.19)\%,$$

which is in substantial disagreement ($\sim 3\sigma$) with the world average value (see Sec. I) of $(1.47 \pm 0.13)\%$, but agrees with the result from the BES collaboration [16]: $\mathcal{B}(J/\psi \rightarrow 3\pi) = (2.10 \pm 0.12)\%$.

IX. SUMMARY

The process $e^+e^- \rightarrow \pi^+\pi^-\pi^0\gamma$ was studied for the 3π invariant masses up to $3 \text{ GeV}/c^2$ and at the J/ψ mass. From the measured 3π mass spectrum we obtained the $e^+e^- \rightarrow \pi^+\pi^-\pi^0$ cross section for the $1.05 < \sqrt{s'} < 3 \text{ GeV}$ energy range. The results are in agreement with the SND measurement [26] for $\sqrt{s'} < 1.4$ and significantly exceed the DM2 data [7] in the $1.4 < \sqrt{s'} < 2.2$ range. The $e^+e^- \rightarrow \pi^+\pi^-\pi^0$ cross section in the energy range up to 1.8 GeV is described well by a sum of the contributions of four isoscalar resonances: ω , ϕ , ω' , and ω'' . From the fit of the 3π mass spectrum we obtained the following parameters for these resonances:

$$\begin{aligned} \mathcal{B}(\omega \rightarrow e^+e^-) \mathcal{B}(\omega \rightarrow 3\pi) &= (6.70 \pm 0.06 \pm 0.27) \times 10^{-5}, \\ \mathcal{B}(\phi \rightarrow e^+e^-) \mathcal{B}(\phi \rightarrow 3\pi) &= (4.30 \pm 0.08 \pm 0.21) \times 10^{-5}, \\ \mathcal{B}(\omega' \rightarrow e^+e^-) \mathcal{B}(\omega' \rightarrow 3\pi) &= (0.82 \pm 0.05 \pm 0.06) \times 10^{-6}, \\ M_{\omega'} &= (1350 \pm 20 \pm 20) \text{ MeV}/c^2, \\ \Gamma_{\omega'} &= (450 \pm 70 \pm 70) \text{ MeV}/c^2, \\ \mathcal{B}(\omega'' \rightarrow e^+e^-) \mathcal{B}(\omega'' \rightarrow 3\pi) &= (1.3 \pm 0.1 \pm 0.1) \times 10^{-6}, \\ M_{\omega''} &= (1660 \pm 10 \pm 2) \text{ MeV}/c^2, \\ \Gamma_{\omega''} &= (230 \pm 30 \pm 20) \text{ MeV}/c^2. \end{aligned}$$

The electronic widths of ω' and ω'' corresponding to these resonance parameters, $\Gamma(\omega' \rightarrow e^+e^-) \approx 370 \text{ eV}$ and $\Gamma(\omega'' \rightarrow e^+e^-) \approx 570 \text{ eV}$, are comparable with the $\omega(782)$ electronic width, in disagreement with expectations of the quark model (see, for example, Ref. [34]).

From the measured number of events in the $e^+e^- \rightarrow J/\psi\gamma \rightarrow \pi^+\pi^-\pi^0\gamma$ reaction we determine

$$\begin{aligned} \Gamma(J/\psi \rightarrow e^+e^-) \mathcal{B}(J/\psi \rightarrow 3\pi) \\ = (0.122 \pm 0.005 \pm 0.008) \text{ keV.} \end{aligned}$$

Dividing this value by $\Gamma(J/\psi \rightarrow e^+e^-) = (5.61 \pm 0.20)$ keV [8] we obtain $\mathcal{B}(J/\psi \rightarrow 3\pi) = (2.18 \pm 0.19)\%$, which is in $\sim 3\sigma$ disagreement with the world average value of $(1.47 \pm 0.13)\%$ (see Sec. I), but agrees with the recent result from the BES Collaboration [16]: $(2.10 \pm 0.12)\%$.

X. ACKNOWLEDGMENTS

We are grateful for the extraordinary contributions of our PEP-II colleagues in achieving the excellent luminosity and machine conditions that have made this work possible. The success of this project also relies critically on the expertise and dedication of the computing organizations that support *BABAR*. The collaborating institutions wish to thank SLAC for its support and the kind hospitality extended to them. This work is sup-

ported by the US Department of Energy and National Science Foundation, the Natural Sciences and Engineering Research Council (Canada), Institute of High Energy Physics (China), the Commissariat à l'Energie Atomique and Institut National de Physique Nucléaire et de Physique des Particules (France), the Bundesministerium für Bildung und Forschung and Deutsche Forschungsgemeinschaft (Germany), the Istituto Nazionale di Fisica Nucleare (Italy), the Foundation for Fundamental Research on Matter (The Netherlands), the Research Council of Norway, the Ministry of Science and Technology of the Russian Federation, and the Particle Physics and Astronomy Research Council (United Kingdom). Individuals have received support from CONACyT (Mexico), the A. P. Sloan Foundation, the Research Corporation, and the Alexander von Humboldt Foundation.

-
- [1] A.B. Arbuzov *et al.*, JHEP **9812**, 009 (1998).
 - [2] S. Binner, J.H. Kuhn, and K. Melnikov, Phys. Lett. B **459**, 279 (1999).
 - [3] M. Benayoun *et al.*, Mod. Phys. Lett. A **14**, 2605 (1999).
 - [4] KLOE Collaboration, A. Aloisio *et al.*, submitted to Phys. Lett. B, hep-ex/0407048.
 - [5] Review of Particle Physics, S. Eidelman *et al.*, Phys. Lett. B **592**, 1 (2004).
 - [6] SND Collaboration, M.N. Achasov *et al.*, Phys. Rev. D **66**, 032001 (2002).
 - [7] DM2 Collaboration, A. Antonelli *et al.*, Z. Phys. C **56**, 15 (1992).
 - [8] *BABAR* Collaboration, B. Aubert *et al.*, Phys. Rev. D **69**, 011103 (2004).
 - [9] B. Jean-Marie *et al.*, Phys. Rev. Lett. **36**, 291 (1976).
 - [10] W. Bartel *et al.*, Phys. Lett. B **64**, 483 (1976).
 - [11] DASP Collaboration, R. Brandelik *et al.*, Phys. Lett. B **74**, 292 (1978).
 - [12] PLUTO Collaboration, G. Alexander *et al.*, Phys. Lett. B **72**, 493 (1978).
 - [13] M.E.B. Franklin *et al.*, Phys. Rev. Lett. **51**, 963 (1983).
 - [14] MARK-III Collaboration, D. Coffman *et al.*, Phys. Rev. D **38**, 2695 (1988).
 - [15] BES Collaboration, J.Z. Bai *et al.*, Phys. Rev. D **54**, 1221 (1996).
 - [16] BES Collaboration, J.Z. Bai *et al.*, Phys. Rev. D **70**, 012005 (2004).
 - [17] *BABAR* Collaboration, B. Aubert *et al.*, Nucl. Instr. and Meth. A **479**, 1 (2002).
 - [18] H. Czyz and J.H. Kuhn, Eur. Phys. J. C **18**, 497 (2001).
 - [19] M. Caffo, H. Czyz, and E. Remiddi, Nuo. Cim. **110A**, 515 (1997); Phys. Lett. B **327**, 369 (1994).
 - [20] E. Barberio and Z. Was, Comput. Phys. Commun. **79**, 291 (1994).
 - [21] G. Rodrigo, H. Czyz, J.H. Kuhn, and M. Szopa, Eur. Phys. J. C **24**, 71 (2002).
 - [22] T. Sjostrand, Comput. Phys. Commun. **82**, 74 (1994).
 - [23] S. Jadach and Z. Was, Comput. Phys. Commun. **85**, 453 (1995).
 - [24] S. Agostinelli *et al.*, Nucl. Instr. and Meth. A **506**, 250 (2003).
 - [25] SND Collaboration, M.N. Achasov *et al.*, Phys. Rev. D **68**, 052006 (2003).
 - [26] SND Collaboration, M.N. Achasov *et al.*, Phys. Rev. D **65**, 032002 (2002).
 - [27] KLOE Collaboration, A. Aloisio *et al.*, Phys. Lett. B **561**, 55 (2003).
 - [28] Crystal Ball Collaboration, Z. Jakubowski *et al.*, Z. Phys. C **40**, 49 (1988).
 - [29] CMD-2 Collaboration, R.R. Akhmetshin *et al.*, Phys. Lett. B **476**, 33 (2000); the results were corrected in Phys. Lett. B **578**, 285 (2004).
 - [30] A.B. Clegg and A. Donnachie, Z. Phys. C **62**, 455 (1994).
 - [31] CMD-2 Collaboration, R.R. Akhmetshin *et al.*, Phys. Lett. B **489**, 125 (2000).
 - [32] Crystal Barrel Collaboration, A.V. Anisovich *et al.*, Phys. Lett. B **485**, 341 (2000).
 - [33] E852 Collaboration, P. Eugenio *et al.*, Phys. Lett. B **497**, 190 (2001).
 - [34] S. Godfrey and N. Isgur, Phys. Rev. D **32**, 189 (1985).
 - [35] MARK-III Collaboration, L. Chen and W.M. Dunwoodie, in *Proceedings of Hadron 91 Conference, College Park, MD, 1991*, p. 100, SLAC-PUB-5674 (1991).